Inverse Compensation of Hysteresis using Modified Generalized Prandtl-Ishlinskii Hysteresis Model

Wenjun Ye

A Thesis

in

The Department

of

Mechanical and Industrial Engineering

Presented in Partial Fulfillment of the Requirements

for the Degree of

Master of Applied Science (Mechanical Engineering) at

Concordia University

Montréal, Québec, Canada

September 2016

CONCORDIA UNIVERSITY

School of Graduate Studies

This is to certify that the thesis prepared

By: **Wenjun Ye**

Entitled: **Inverse Compensation of Hysteresis using Modified Generalized Prandtl-Ishlinskii Hysteresis Model**

and submitted in partial fulfillment of the requirements for the degree of

Master of Applied Science (Mechanical Engineering)

complies with the regulations of this University and meets the accepted standards with respect to originality and quality.

Signed by the Final Examining Committee:

_____ Chair
Dr. Mingyuan Chen

_____ External Examiner
Dr. Wei-Ping Zhu

_____ Examiner
Dr. Subbash Rakheja

_____ Supervisor
Dr. Chun-Yi Su

Approved by _____
Martin D. Pugh, Chair
Department of Mechanical and Industrial Engineering

_____ 2016

_____
Amir Asif, Dean
Faculty of Engineering and Computer Science

Abstract

Inverse Compensation of Hysteresis using Modified Generalized Prandtl-Ishlinskii Hysteresis Model

Wenjun Ye

Smart material based actuators, due to their properties of high precision, fast response, high power density, and small sizes, have become ideal actuators in many industrial applications, i.e. micro positioning, atomic force microscopy, and so forth. However, these smart actuators exhibit hysteresis nonlinear effects, which may worsen tracking performances, lead oscillations or even instabilities. Therefore, the existence of the hysteresis nonlinearities limits the utilization of smart material based actuators, and became the bottleneck of the control strategies development for systems with the smart actuators.

In order to overcome the effects of the hysteresis, a number of hysteresis models have been proposed in the literatures. Among them, the Prandtl-Ishlinskii (PI) model, thanks to its significant analytical invertible property, has become one of the most popular hysteresis models. Nevertheless, the PI model can only describe a kind of symmetric, rate-independent, and non-saturated hysteresis, which restricts the use of PI model. Therefore, it requires to generalize the PI model, making it able to represent more complicated hysteresis phenomena, while keeping analytically invertible property.

In this thesis, based on the PI model and the Generalized Prandtl-Ishlinskii (GPI) model available in the literature, a modified Generalized Prandtl-Ishlinskii (mGPI) model is proposed, which aims to redefine the play operator in the GPI so as to describe a kind of asymmetric and saturated hysteresis nonlinearities.

According to the proposed mGPI model, an analytical inverse model is also derived, which can be used as an inverse compensator of the hysteresis nonlinearities. To validated the proposed

inverse model, simulation results are provided confirming the proposed analytical inverse of the mGPI model.

Acknowledgments

I would like to express my gratitude to my supervisor, Dr. Chun-Yi Su, for his professional supervision, insightful guidiance, and constant help thoughout the years.

I would also like to thank my colleagues and friends: Dr Zhi Li and Mr. Hou-Pin Yoong for their kindly help.

Last but not least, I would like to acknowledge my parents for their support.

Contents

List of Figures

List of Tables

Chapter 1

Introduction

1.1 Motivation

In recent decades, due to the increasing demands of precision of actuators in various industrial applications, smart material based actuators, because of its excellent performances, such as high resolution and fast response, smart material becomes an ideal material for high precision actuators. Unfortunately, the smart material based actuators exhibit hysteresis nonlinearity, a highly nonlinear effect which is multi-valued, with memory effect, various, and non-smooth [1], as illustrated by Fig. 1.1.

This nonlinearity extremely restricts the utilization of smart material based actuators. Different from the traditional controller structure, the control system with smart material actuators proceeds a hysteresis nonlinearity part with the controlled plant. Thus, the hysteresis nonlinearity and controlled plant are coupled together, as shown in Fig. 1.2. Therefore, the output of hysteresis not measurable, which makes the control more challenging. The embedded hysteresis effect may cause poor precisions, oscillations, and even instabilities [2].

In order to alleviate the drawbacks caused by hysteresis effect, mathematical models which can describe the characters of hysteresis nonlinearities become necessary. In [3], some popular mathematical models of hysteresis nonlinearities were surveyed . The most cited models are Duhem model [4], Preisach model [5], Krasnoselskii-Pokrovskii (KP) model [6], and Prandtl-Ishlinskii PI model [7]. Among these models, PI model is only one with analytical inverse property [8]. With this

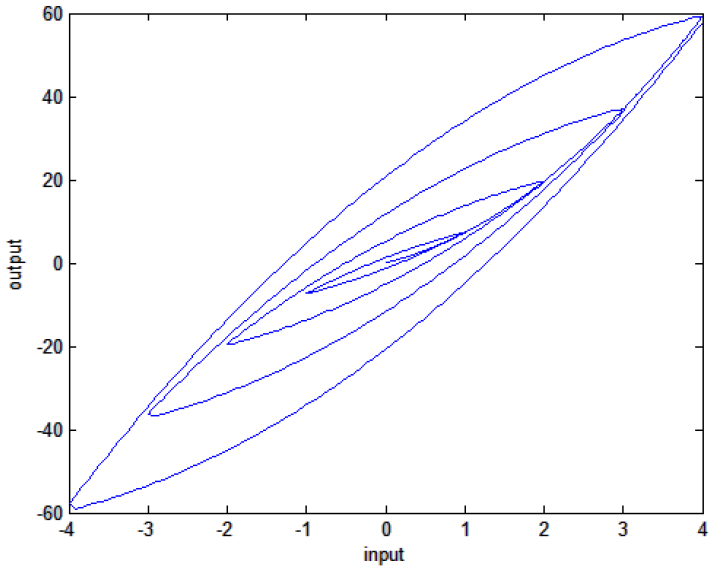

Figure 1.1: Hysteresis Nonlinearity

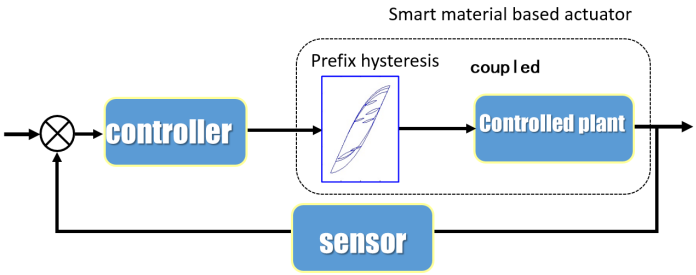

Figure 1.2: Structure of Control System Using Smart Material Based Actuators

significant property, an inverse compensator can be used to eliminate the hysteresis nonlinearity in control system. Nevertheless, the use of the PI model is highly limited because it can only describe one type of hysteresis nonlinearities which are symmetric, rate-independent, and non-saturated.

In recent years, generalizing the PI model became a topic of hysteresis research, several works have been present to extend the application range of the PI model while keeping it invertible property. Notably, a generalized Prandtl-Ishlinskii (GPI) model has been proposed in [9], which can describe a more general class of hysteresis, and its inverse has been proposed in [10]. However, this GPI model can be seen as cascades of envelop functions and PI models, its application range is still limited. A modification of GPI model and the derivation of its inverse are requested.

1.2 Objective of the Thesis

In order to compensate the hysteresis nonlinearities in the smart material based actuators, a number of hysteresis models are proposed. They can be classified into two classes: physics-based models and phenomenological models.

The physic-based models are based on the element physical properties of a particular kind of materials. They are complicated and can not precisely describe the hysteresis nonlinearities of the other materials. The phenomenological models, which describe the hysteresis by the input-output relations, are utilized to characterize the hysteresis. Based on the mathematical tools they use, they can be categorized into three kinds, differential-equation-based models, operator-based models, and other models. The differential-equation-based models are also very complicated, whose general solutions are still not available. Among the operator-based models, the Prandtl-Ishlinskii (PI) model, because of its analytical invertible property, became one of the most popular hysteresis models. However, it can only describe a kind of hysteresis. Recent efforts have been paid on generalizing the PI model, making it able to describe a wider range of hysteresis, while keeping it invertible.

In this thesis, based on the PI model, together with its generalization, some analysis and modification will be addressed. The objective of the thesis is to improve the Generalized PI (GPI) model, making it able to descirbe hysteresis precisely, and also provided the inverse of the modified GPI model.

1.3 Contributions

This thesis focuses on the modeling and compensation of the hysteresis nonlinearities in control systems, especially systems with smart material based actuators. In this thesis, based on the available Prandtl-Ishlinskii (PI) model and the Generalized Prandtl-Ishlinskii (GPI) model in the literatures, a modified Generalized Prandtl-Ishlinskii (mGPI) model is presented . Subsequently, an inverse compensator based on the proposed mGPI model is derived and validated. The main contributions of the thesis are as follows,

- In Chapter 3, the limitations of the PI model and the GPI model are addressed. Based on these

models, a modified Generalized Prandtl-Ishlinskii (mGPI) model is provided. Compared with the PI model, the mGPI model can characterize a more general class of the hysteresis nonlinearities. Compared with the GPI model, the mGPI model has several advantages. For instance, 1) the threshold of the modified generalized play operator is $\pm r$, independent from the envelop functions $\gamma[v]$; 2) the modified generalized play operator can inherit the bounds of the envelop function, which makes sense when modeling saturated hysteresis; 3) the operators in the GPI model will stop functioning with some envelop functions and threshold, in contrast, the operators in the proposed mGPI model will always work with any input; 4) the mGPI model is not simply the cascade of a preprocessing $\gamma[v]$ and a classical PI model, which is more useful in hysteresis modeling.

- In Chapter 4, based on the proposed mGPI model, an analytical inverse is derived, which can be used as an feed-forward compensator of the hysteresis nonlinearities. Subsequently, the numerical implementation methods are provided. Following these steps, the parameters of the proposed inverse compensator can be calculated.

- In Chapter 5, to validate the proposed inverse compensator, simulation results are provided. An identity function, a linear function, and a nonlinear function are chosen, respectively, as the envelop functions, to generate the mGPI model. The inverse compensator are constructed accordingly. Illustrated by the simulation results, the proposed model can precisely describe the hysteresis nonlinearities and the derived inverse compensator can effectively cancel the nonlinear effects caused by hysteresis.

1.4 Organization of the Thesis

The thesis consists of 6 chapters including the introductions Chapter 1. The topics of rest chapters are as follows.

Chapter 2: A literature review of hysteresis, and existing control approach dealing with hysteresis nonlinearities will be presented.

Chapter 3: A detailed review of the PI model, its hysteresis operators, and the GPI model will be

provided. Subsequently, a modified GPI (mGPI) model will be proposed, which can describe a larger class of hysteresis effects.

Chapter 4: The analytical inverse of the proposed mGPI model will be derived, which can be used as the inverse compensator of the mGPI model. The numerical implementation method of the proposed inverse model will be provided.

Chapter 5: The proposed mGPI model and its inverse compensator will be simulated with different kinds of envelop functions. The effectiveness of the model and the compensator will be validated by the simulation results.

Chapter 6: Conclusions and future works will be included.

Chapter 2

Literature Review

In this chapter, an comprehensive literature review of hysteresis phenomenon, hysteresis models, and the control approaches will be provided.

2.1 Hysteresis Nonlinearity

Hysteresis effects widely exist in many in areas. Mathematician I. D. Mayergoyz provides mathematical description of hysteresis in [3]. One popular scientific definition of the hysteresis is introduced by the Scottish physicist, Alfred Ewing [6], as follows,

Hysteresis: When there are two quantities M and N, such that cyclic variations of N cause cyclic variation of M, then if the changes of M lag behind those of N, we may say that there is hysteresis in the relation of M and N.

Generally, when speaking hysteresis, it also requires the nonlinear behaviors with the following essential properties.

Multivalued: With the same input signal, the output of the system may be various, and vice versa.

Wiping Out: The wiping out property is that the ouput of the hysteresis is only related to the current input and the history of the output, while all other inputs are wiped out.

Congruent Minor Loop: The congruent minor loop property means that the minor loops caused by the same input need to be congruent.

Above properties can be observed from the Fig. 2.1.

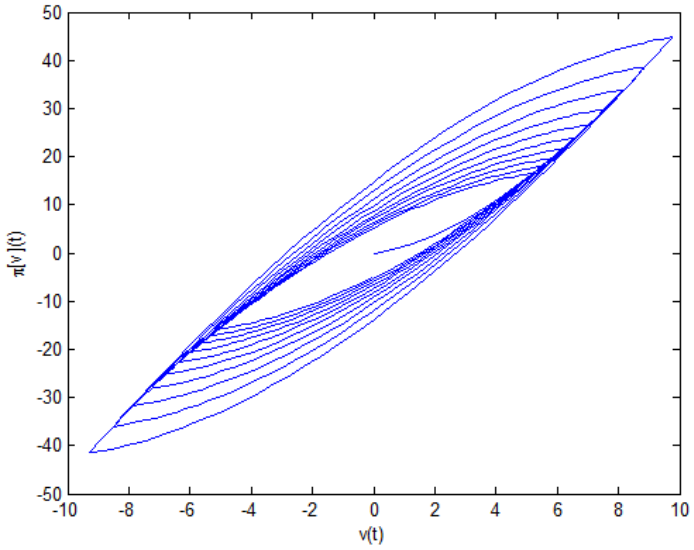

Figure 2.1: A Typical hysteresis behavior under input $v(t) = 10sin(2\pi t)/(1 + 0.1t)$, $t \in [0, 10]$, with properties of multivalued, wiping out, and congruent minor loop.

2.2 Hysteresis Models

Hysteresis nonlinearities widely exist in smart material based actuators. These nonlinear effects have become the bottleneck of controller designs, because the nonlinearity is coupled with controlled plant, making the outputs of the nonlinearities not measurable. In order to alleviate the drawbacks of the hysteresis nonlinearities, hysteresis models are requested.

According to references, the proposed hysteresis models can be classified into two types, physics-based models and phenomenological models [11]. The physics-based models are developed on physical phenomena and principles. These models include JilesAtherton (J-A) model [12], domain wall model [13], and so forth. The phenomenological models, in contrast, are proposed to describe the hysteresis nonlinearities phenomena without providing detailed physical principles. The phenomenological models can classified into differential-equation-based models, operator-based

models, and other models, depend on their related mathematical tools. Fig. 2.2 describes the classifications of hysteresis models.

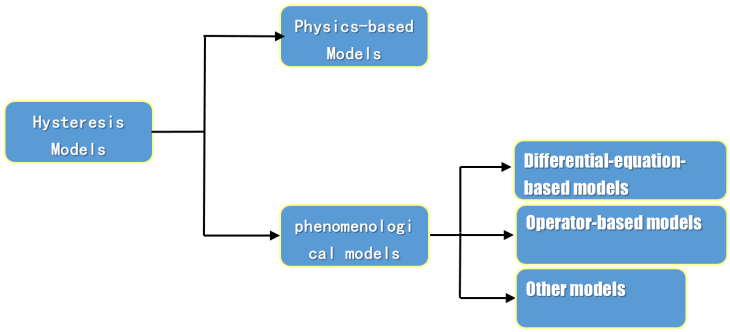

Figure 2.2: Category of hysteresis models

2.2.1 Physics-based Models

The physics-based models are built on physical phenomena and first principles. The JilesAtherton (J-A) model [12] is one of the most famous physics-based hysteresis models. It is based on the physical properties of ferromagnetic hysteresis. The J-A model is widely used in ferromagnetic hysteresis modeling, thanks to its ability to describe main features of hysteresis nonlinearities of ferromagnetic materials. Another famous physics-based hysteresis model is domain wall model [13]. The domain wall model is used to describe the piezoelectric actuator hysteresis nonlinearities with an ordinary differential equation.

However, these physics-based models are normally very complicated, because these models concern so many physical details. Besides, these models are material- specific, which means a model developed on one material can hardly be used on another kind of materials. Thus, the industrial applications of physics-based models are quite limited.

2.2.2 Phenomenological Models

The phenomenological models, in contrast to the physics-based models, are proposed to describe the hysteresis nonlinearities phenomena without introducing detailed physical meanings. As illustrated in Fig. 2.3, the phenomenological hysteresis models can be classified into 3 classes,

differential-equation-based models, operator-based models, and other hysteresis models, based on the mathematical tools used in models.

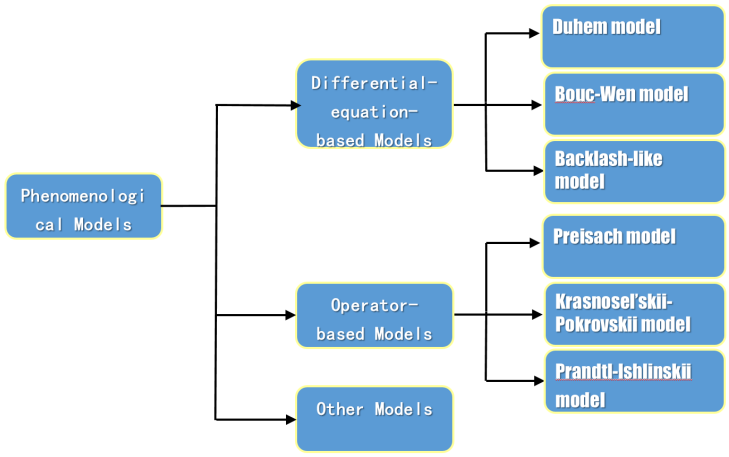

Figure 2.3: Category of phenomenological hysteresis models

Differential-equation-based Models: The differential-equation-based models present the hysteresis nonlinearities description with differential equations [14]. The most popular differential-equation-based hysteresis models are Duhem model, Bouc-Wen model, and Backlash-like model.

Duhem Model: The Duhem model was proposed to describe the magnetic hysteresis nonlinearities [15], by depicting the hysteresis effect of a mass-spring-damper system. It can also present hysteresis of other smart materials. In Duhem model, the input v and output w of hysteresis can be described as [15]:

$$\dot{w}(t) = f_1(w(t), v(t))\dot{v}_+(t) - f_2(w(t), v(t))\dot{v}_-(t) \tag{1}$$

where

$$\begin{cases} v_+ = \frac{|v|+v}{2} \\ v_- = \frac{|v|-v}{2} \end{cases} \tag{2}$$

f_1 and f_2 are the shape functions related to both input and output of hysteresis.

Bouc-Wen model: Bouc-Wen model is a semi-physical model based on Duhem model(1). It was proposed by Bouc and later generalized by Wen [16]. In Bouc-Wen model, the hysteresis input

v and output w are presented as:

$$\dot{w} = A\dot{v} - \beta\dot{v}|w|^n - \alpha|\dot{v}||w|^{n-1}w \tag{3}$$

where A, α, and β are shape parameters [17].

Backlash-like model: To introduce backlash-like model, a simplified Duhem model needs to be provided.

$$\frac{dw}{dt} + a|\frac{dv}{dt}|g(v,w) = b\frac{dv}{dt} \tag{4}$$

On the basis of simplified Duhem model (4), a backlash-like model was proposed [18], describing the hysteresis nonlinearities as:

$$\frac{dw}{dt} = \alpha|\frac{dv}{dt}|[cv - w] + B_1\frac{dv}{dt} \tag{5}$$

where α, c and B_1 are shape parameters. In [18], an explicit solution was provided as,

$$w(t) = cv(t) + d(v(t)) \tag{6}$$

With this model, traditional robost controller can be used to compensate the hysteresis nonlinearities without building the hysteresis inverse.

In conclusion, with differential-equation-based models, the hysteresis nonlinearities can be presented in a first-order differential equation. However, it is hard to get the analytical solution of these equations, the inverse compensator of hysteresis nonlinearities based on differential-equation-based hysteresis models is still not available.

Operator-based models: Operator-based hysteresis models are a kind of models describing hysteresis nonlinearities with the integral of hysteresis operators [6]. Currently, they are the most popular hysteresis models in industrial applications, especially in smart material actuators. Based on the hysteresis operators utilized, the operator-based models include the Preisach model [5], Krasnoselskii-Pokrovskii (KP) model [6], and Prandtl-Ishlinskii PI model [7].

Preisach Model: The Preisach model is a hysteresis model based on relay operator. As depicted in Fig.2.4, the relay operator $\hat{\gamma}_{\alpha\beta}[v(t)]$ is characterized by two threshold $\alpha > \beta$ and two outputs $+1$ and -1. The output $w(t)$ keeps constant until the input value $v(t)$ crosses the threshold α from below or β from above.

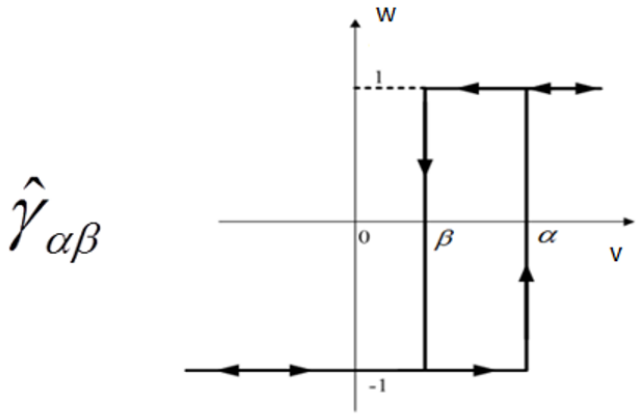

Figure 2.4: Relay Operator

The Preisach model describes hysteresis as [6],

$$w(t) = P[v](t) = \int\int_{\beta\leq\alpha} \mu(\alpha,\beta)\hat{\gamma}_{\alpha\beta}[v(t)]d\alpha d\beta \tag{7}$$

where$\mu(\alpha,\beta)$ is called the weight function or the density function, as Fig. 2.5 shows.

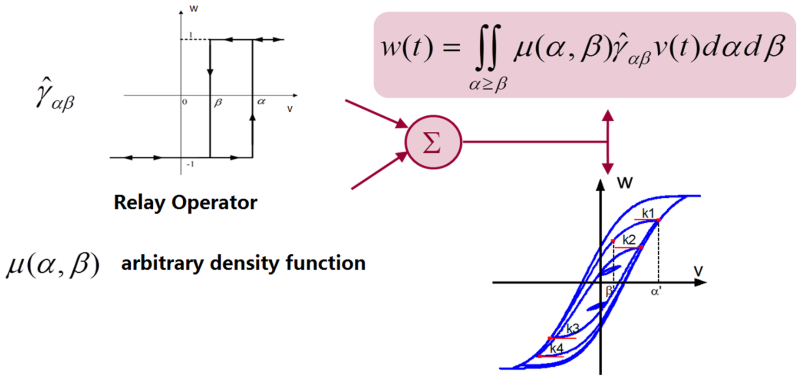

Figure 2.5: Preisach Model

Due to the double integral, both the parameter identification and the inverse construction are very difficult. Besides, the control signal v is included in the integral, which makes the controller design become challenge.

Krasnoselskii-Pokrovskii (KP) Model: Similar to Preisach model, Krasnoselskii-Pokrovskii (KP) model is a hysteresis model based on the KP operator $k_p[v, \xi(\rho)]$, which can be treated as a generalization of relay operator [6]. As illustrated by Fig. 2.6, KP model is also the double integral of related KP operator,

$$w(t) = \Lambda[v](t) = \int \int_{\rho_2 \geq \rho_1} \mu(\rho_2, \rho_1) k_p[v, \xi(\rho)](t) d\rho_2 d\rho_1 \tag{8}$$

where $\mu(\rho_2, \rho_1)$ is the density function, $\rho = (\rho_2, \rho_1)$. Due to the similar structure of Preisach model, KP model is also with the characteristics of non-invertible, control signal included in integral, and so forth.

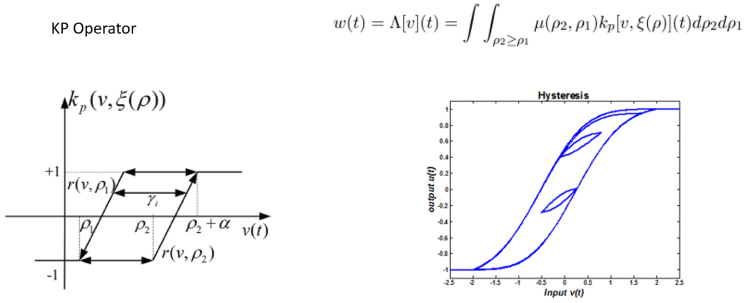

Figure 2.6: Krasnoselskii-Pokrovskii (KP) model

Prandtl-Ishlinskii PI Model: Prandtl-Ishlinskii PI model is developed by introducing play operator $F_r[v](t)$ or stop operator $E_r[v](t)$ [15] [19]. Using play operator as an example, as illustrated by Fig. 2.7, the output of play operator can be defined as,

$$\begin{cases} w(0) = F_r[v](0) = f_r(v(0), 0) \\ w(t) = F_r[v](t) = f_r(v(t), w(t_i)), \quad for\ t_i < t \leq t_{i+1},\ 0 \leq i \leq N-1 \end{cases} \tag{9}$$

with

$$f_r(v, w) = max\{v - r, min\{v + r, w\}\} \tag{10}$$

where $0 = t_0 < t_1 < \ldots < t_N = t_E$ is a partition of $[0, t_E]$ such that the function v is monotone on each of the subintervals $[t_i, t_{i+1}]$ in [7].

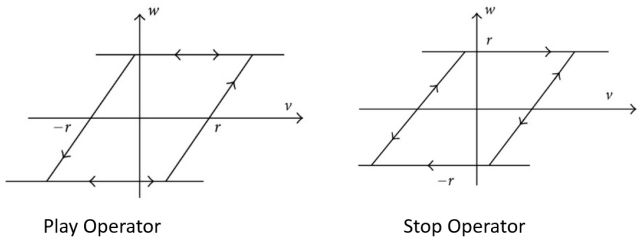

Figure 2.7: Play operator and stop operator

Thus the Play-operator-based PI model is presented as,

$$w(t) = \Pi[v](t) = p_0 v(t) + \int_0^R p(r) F_r[v](t) dr \tag{11}$$

where $p(r)$ is the density function and p_0 is a positive parameter.

A critical advantage of the PI model is that by avoiding the non-differentiable relay operator, the PI model is invertible. In [8], Krejci provided an analytical inverse of the PI model. However, the PI model can only describe a kind of symmetrical and rate-independent hysteresis, current research topics are generalizing the PI model, making it able to describe a more complicated hysteresis while keeping invertible. Since this thesis is dealing with the modified generalized PI model, the detailed properties of the PI model and its generalization will be discussed in the next chapter.

Other Hysteresis Models: Besides the differential-equation-based models and the operator-based models, there are some other phenomenological hysteresis models. Most of these models predict the hysteresis nonlinearities behaviors using intelligent algorithms such as, Neural Network [20] and Support Vector Machine [21]. These models can describe the hysteresis behaviors in some specific fields without using first order differential equations or hysteresis operators, but they are

not as popular as the differential-equation-based models and the operator-based models.

2.3 Compensation of Hysteresis Nonlinearities

Over the past decades, smart material based actuators have widely been used in industrial areas, especially micro-position applications, due to their high precision, fast response, high power density, and small size. However, these smart materials are with a highly nonlinear effect, hysteresis.

This effect becomes the critical limitation of the utilization of smart material based actuators. As illustrated by Fig. 1.2, the hysteresis nonlinearity and the controlled plant are coupled together, making the output of hysteresis not measurable. In this case, traditional controller can not be directly applied on these systems, or the embedded hysteresis nonlinearities may cause poor precisions, oscillations, and even instabilities [2], as shown in Fig. 2.8.

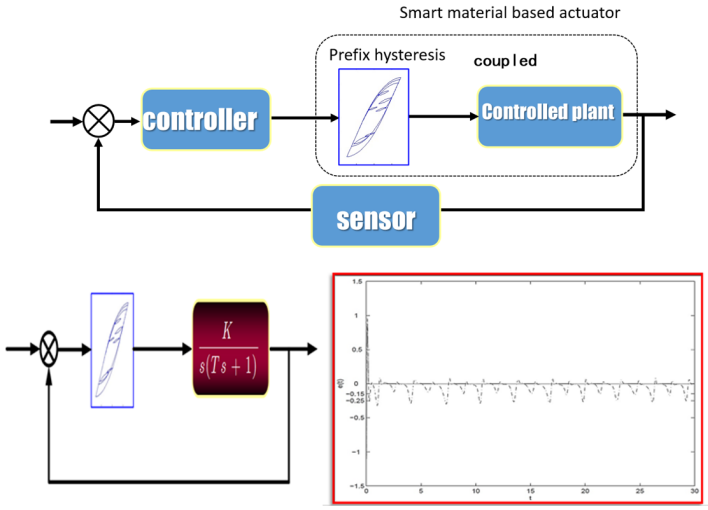

Figure 2.8: Hysteresis nonlinearities limits the controller performance

Therefore, effective approaches to compensate the hysteresis nonlinearities are extremely desired. Existing control approaches treating the hysteresis can be classified into two classes, the inverse-model-based control methods and the direct control methods.

2.3.1 Inverse-model-based Control Methods

The most popular methods to compensate the hysteresis nonlinearities is the inverse-model-based control methods. By constructing the inverse model of hysteresis, the influences of the hysteresis nonlinearities can be reduced or mitigated. After this compensation (cancellation), the traditional control approaches can be utilized for the controller designs. This kind of methods was adopted by Tao and Kokotovic in [2].

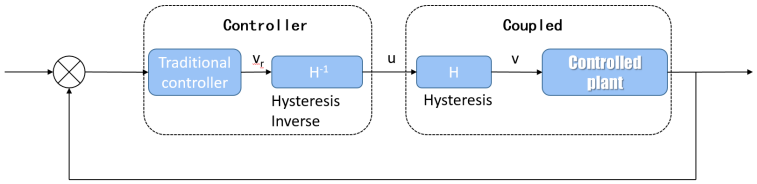

Figure 2.9: Invert-model-based control methods

As depicted by Fig.2.9, an inverse hysteresis model is cascaded between the traditional controller and the hysteresis part. The actual output of the controller $u(t) = H^{-1}[v_c](t)$. Because the smart material based actuators are with the hysteresis effect, the output of the actuator $v(t) = H[u](t)$. Thus, if a precise inverse hysteresis model H^{-1} is available, the output of the actuators is $v(t) = H[u](t) = H \circ H^{-1}[v_c](t) = v_c(t)$. In this way, we can precisely control the output of the actuators $v(t)$, which makes traditional controller effective for the systems with hysteresis.

Inspired by Tao and Kokotovic's work, considerable inverse-model-based hysteresis control methods have been proposed. The main topics of these researches are how to construct mathematically the inverse of these hysteresis models.

Differential-equation-based Models: When the hysteresis is presented by differential-equation-based models, for instance, the Duhem model, the Bouc-Wen model and the Backlash-like model, because of the complexity of the models and the unknown of the equation solutions, the construction of the inverse models is extremely difficult or even impossible. Therefore, among those hysteresis models discussed in Section 2.2, construction of inverse hysteresis models is mainly for operator-based models, such as the Preisach and PI models.

Operator-based Models: It is mentioned that there is no analytical inverse for the Preisach model and the KP model. Therefore, approximate inverse of Preisach model by numerical methods are adopted by researchers.

(1) In [22], based on the Preisach model, Ge and Journeh presented a computer-based tracking control approach for a piezoceramic actuator.

(2) In [23], Tan and Baras proposed a parameter identification methods for Preisach model and related inverse control approach.

(3) In [24], Song et al. derived a numerical inverse Preisach model, and achieved tracking control of a Piezoceramic Actuator.

(4) In [25], Iyer et al. introduced the concept of regularization to study the properties of approximate inverse schemes for the Preisach operator. Then, presented the fixed point and closest-match algorithms for approximately inverting the Preisach operator.

Varying from the Preisach mode and KP model, the PI model is analytical invertible. In [8], Kerjci and Kuhnen provided the the analytical inverse. With this significant advantage, considerable research works have been done to extend the PI model, making the extension able to describe more complex hysteresis, while keeping the property of invertibility.

(1) In [26], Gu et al. developed a modified PI model to describe a kind of asymmetric hysteresis, while still utilizes the classical play operator as the elementary operator. The related inverse compensator was provided and validated.

(2) Janaideh et al. proposed a Generalized PI model which can describe a kind of asymmetric and saturated input-output hysteresis in [9].

(3) In [10], Janaideh et al. provided and validated the inverse compensator of the Generalized PI model above.

2.3.2 Direct Control Mehtods

As mentioned above, because of the complexities of hysteresis nonlinearities and its related models, inverse-model-based control methods met with a lot of challenges. Therefore, besides the inverse-model-based control methods, some researchers also introduced direct control methods against hysteresis nonlinearities. These methods do not need hysteresis inverse model necessarily, which is their significant advantage. Some popular direct control methods are as follows,

(1) Robost Adaptive Control Mehods: In [27], Su et al. proposed an adaptive variable structure control approach, which can achieve a precise trajectory tracking without necessarily constructing a hysteresis inverse.

(2) Optimal Control Methods: In [28], Mayergoyz firstly proposed the optimal control methods in systems with hysteresis. Motivated by his work, Bagagiolo proposed an optimal control method based on the properties of the PI model in [29], Oates and Smith employed optimal theory using a homogenized energy framework in [30], and so forth.

(3) Sliding Mode Control Methods: Based on the assumption that hysteresis loop is bounded, sliding mode control methods are also employed by researches to deal with systems with hysteresis, i.e. [31]. However, because of ignoring the details and properties of hysteresis nonlinearities, the precisions of this kind of methods are poor.

Chapter 3

Modified Generalized Prandtl-Ishlinskii (mGPI) Model

Smart material based actuators exhibit a highly nonlinear effect, hysteresis. This effect will limit the utilization of smart material based actuators, may cause poor precision, oscillation, or even instability. In order to overcome this annoying nonlinear effect, hysteresis models are highly desired. The PI model, due to its significant property of owning the analytical inverse, became the most popular hysteresis model.

In this chapter, two types of hysteresis operator employed by the PI model, play operator and stop operator, will be introduced firstly. Subsequently, the detailed properties of the PI model and Generalized PI model will be provided. Finally, a Modified Generalized PI model will be proposed and compared with the models above.

3.1 Play Operator and Stop Operator

The Prandtl-Ishlinskii (PI) model is an operator-based hysteresis model. Operator-based hysteresis models are kinds of models with an integral of weighed elementary hysteresis operators. The elementary hysteresis operators PI model uses are the play operator and the stop operator.

3.1.1 The Play Operator

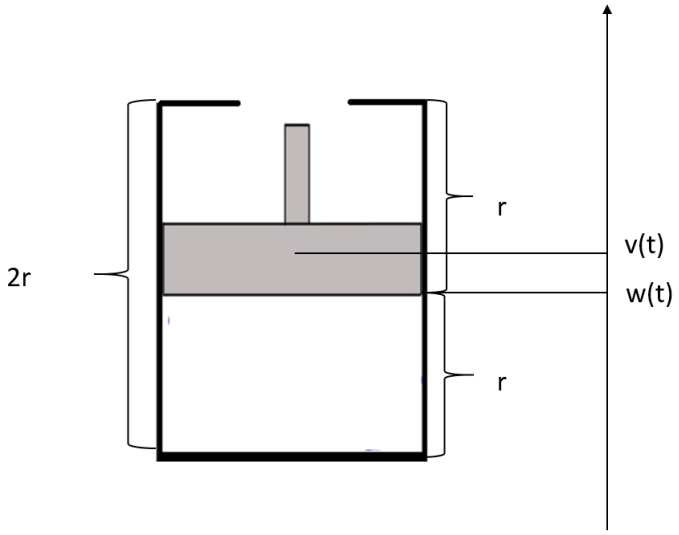

Figure 3.1: Play between cylinder and piston with one DOF

As an example, the play operator can be considered as a relationship between two mechanical elements, a cylinder and a piston, in one Degree of Freedom (DOF), as illustrated by Fig. 3.1. The position of the moving piston $v(t)$ is the input, and the position of the cylinder $w(t)$ is the output. The output $w(t)$ remains constant when the input $v(t)$ moves in the interior, and it will change as $\dot{w}(t) = \dot{v}(t)$ when the piston $v(t)$ hits the boundary of the cylinder$\pm r$. $2r$ denotes the length of the cylinder, which is called the threshold of the play operator.

Thus, for $r \geq 0$, the play operator $w(t) = F_r[v](t)$ can be defined as

$$\begin{cases} w(0) = F_r[v](0) = f_r(v(0), 0) \\ w(t) = F_r[v](t) = f_r(v(t), w(t_i)), \quad for\ t_i < t \leq t_{i+1},\ 0 \leq i \leq N-1 \end{cases} \tag{12}$$

with

$$f_r(v, w) = max\{v - r, min\{v + r, w\}\} \tag{13}$$

where $0 = t_0 < t_1 < \ldots < t_N = t_E$ is a partition of $[0, t_E]$ such that the function v is monotone on each of the subintervals $[t_i, t_{i+1}]$ in [7]. The input-output relationship is depicted in Fig. 3.2.

Some of the key properties of the play operator can be described as follows:

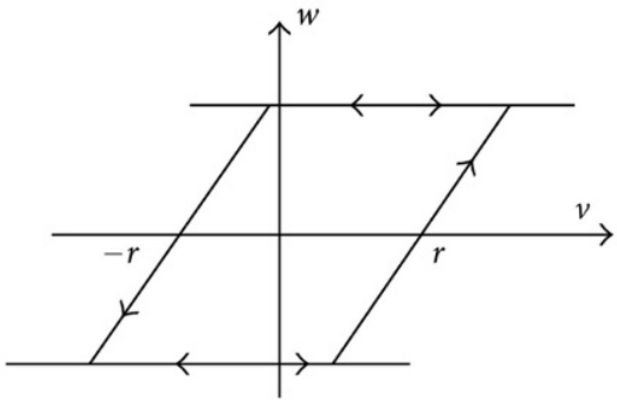

Figure 3.2: Behavior of play operator

- Lipschitz-continuity. Different from the relay operator, for a given input $v(t)$, the play operator is Lipschitz-continues [6].

- Rate-independence. The play operator meet the definition of a rate-independent function in [6],

$$F_r[v \circ \phi] = F_r[v] \circ \phi \tag{14}$$

  where ϕ is an admissible time transformation, i.e. a continuous increasing function $\phi : [0, t_E] \to [0, t_E]$ satisfying $\phi(0) = 0$ and $\phi(t_E) = t_E$.

- Counter-clockwise. As shown in Fig. 3.2, the input-output trajectory of the play operator is counter-clockwise.

3.1.2 The Stop Operator

Similarly, the stop operator can also be considered as a relationship between two mechanical elements, a rod and a piston, in one Degree of Freedom (DOF), as illustrated by Fig. 3.3. The position of the moving rod $v(t)$ is the input, and the position fo the piston $w(t)$ is the output. It is assumed that the piston moves together with the rod, $\dot{w}(t) = \dot{v}(t)$, until the piston $w(t)$ hits the boundary of the cylinder $\pm r$. The output position of the piston $w(t)$ remains constant when the position of the rod $v(t)$ goes away from the cylinder.

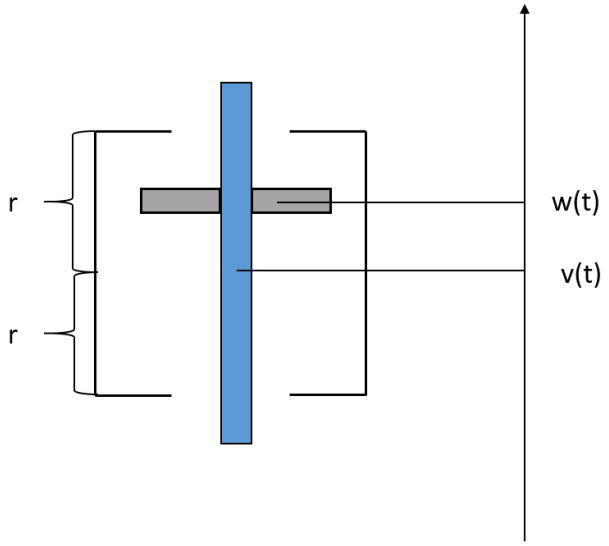

Figure 3.3: Stop between rod and piston with one DOF

Then, for $r \geq 0$, the stop operator $w(t) = E_r[v](t)$ can be defined as

$$\begin{cases} w(0) = E_r[v](0) = e_r(v(0), 0) \\ w(t) = E_r[v](t) = e_r(v(t) - v(t_i) + w(t_i)), \quad for\ t_i < t \leq t_{i+1},\ 0 \leq i \leq N-1 \end{cases} \tag{15}$$

with

$$e_r(v) = min\{r, max\{-r, v\}\} \tag{16}$$

where $0 = t_0 < t_1 < \ldots < t_N = t_E$ is a partition of $[0, t_E]$ such that the function v is monotone on each of the subintervals $[t_i, t_{i+1}]$ in [7]. The input-output relationship of the stop operator is illustrated in Fig. 3.2.

Because the input-ouput relation ship is similar to the stress-strain relationship, the stop operator is also called one-dimentional elastic-plastic element in some references, i.e. [7].

Some of the key properties of the stop operator can be described as follows:

- Lipschitz-continuity. Similar to the play operator, for a given input $v(t)$, the stop operator is

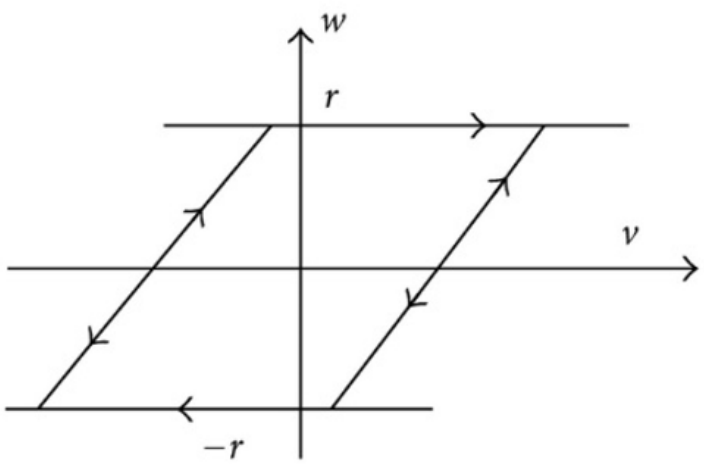

Figure 3.4: Behavior of stop operator (one-dimentional elastic-plastic element)

Lipschitz-continues [6].

- Rate-independence. The stop operator meet the definition of a rate-independent function in [6],

$$E_r[v \circ \phi] = E_r[v] \circ \phi \tag{17}$$

where ϕ is an admissible time transformation, i.e. a continuous increasing function $\phi : [0, t_E] \to [0, t_E]$ satisfying $\phi(0) = 0$ and $\phi(t_E) = t_E$.

- Clockwise. As shown in Fig. 3.4, the input-output trajectory of the stop operator is counter-clockwise.

3.2 Prandtl-Ishlinskii (PI) model

Because the play operator and the stop operator share similar properties, the following of the thesis is focused on the play-operator-based Prandtl-Ishlinskii (PI) model and its generalization.

As mentioned in Section 2.2, the Prandtl-Ishlinskii (PI) model is an operator-based phenomenological hysteresis model. The Play-operator-based PI model is expressed as [7]

$$w(t) = \Pi[v](t) = p_0 v(t) + \int_0^R p(r) F_r[v](t) dr \tag{18}$$

where $p(r)$ is the density function and p_0 is a positive parameter. Because $p(r)$ vanished when r is sufficiently large, a threshold R is chosen as the upper limit of the integral [27].

As an illustration, in Fig. 3.5, the input-output relationship of a PI model with $p_0 = 1$ and $p(r) = e^{-0.001r}$ is provided, with initial value $w(0) = 0$.

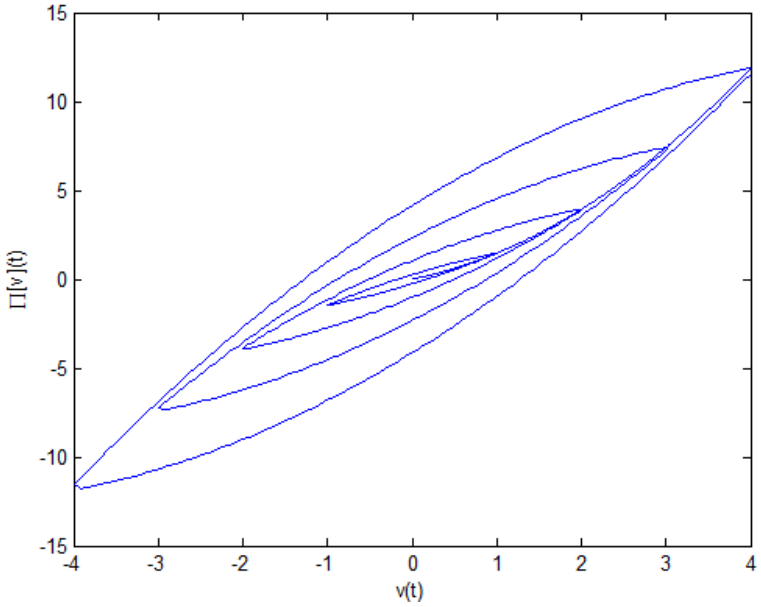

Figure 3.5: Input-ouput relationship of PI model

3.3 Generalized Prandtl-Ishlinskii (GPI) Model

Although the Prandtl-Ishlinskii (PI) model is widely used in hysteresis nonlinearities modeling, according to the descriptions in the previous section, it can only represent a certain kind of symmetric, rate-independt, and non-saturated hysteresis. In order to overcome the limitation of the PI model, in [9], a Generalized PrandtlIshlinskii (GPI) model was proposed. Compared with the classical PI model, the proposed GPI model can describe the asymmetric or saturated hysteresis nonlinearities more effectively. Different from the classical PI model, the GPI model is based on the generalized play operator instead of the traditional play operator.

3.3.1 Generalized Play Operator

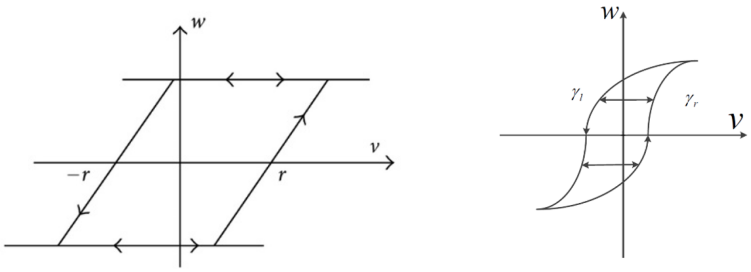

(a) classical play operator (b) generalized play operator

Figure 3.6: Input-output relationships of classical and generalized play operator

As depicted in Fig. 3.6, unlike the classical play operator, the output $w(t)$ increases or decreases with the input $v(t)$ along the curves, γ_l and γ_r, which are called the envelop functions, instead of two straight lines. Therefore, the generalized play operator can describe more classes of hysteresis shapes with the multiple choices of the envelop functions.

For any input $v(t) \in C_m[0, t_E]$, where C_m denotes piecewise monotone functions space, such that the function v is monotone on each of the subintervals $[t_i, t_{i+1}]$ for any $0 = t_0 < t_1 < \ldots < t_N = t_E$ is a partition of $[0, t_E]$ [7], the generalized play operator F_{lr}^{γ} can be analytically defined as [9],

$$\begin{cases} F_{lr}^{\gamma}[v](0) = f_{lr}^{\gamma}(v(0), 0) = w(0) \\ F_{lr}^{\gamma}[v](t) = f_{lr}^{\gamma}(v(0), w(t_i)) \end{cases} \tag{19}$$

with

$$f_{lr}^{\gamma}(v, w) = max\{\gamma_l(v) - r, min\{\gamma_r(v) + r, w\}\} \tag{20}$$

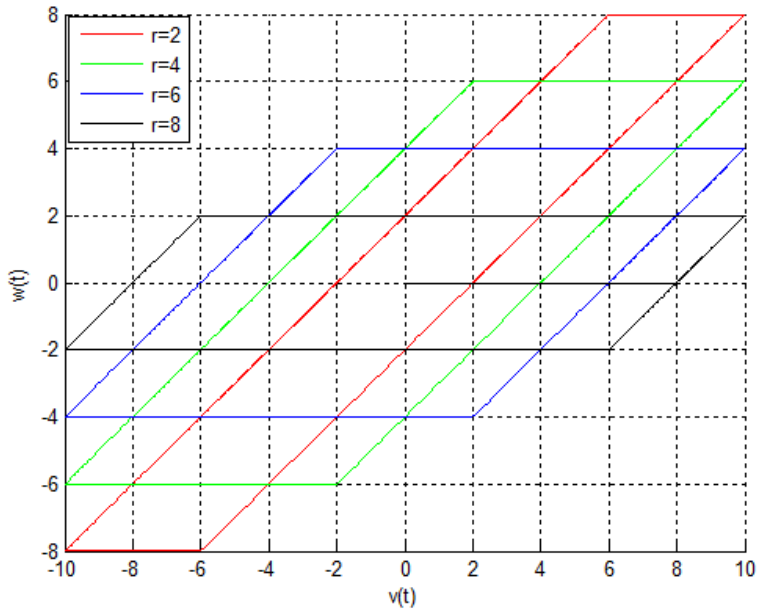

(a) classical play operator

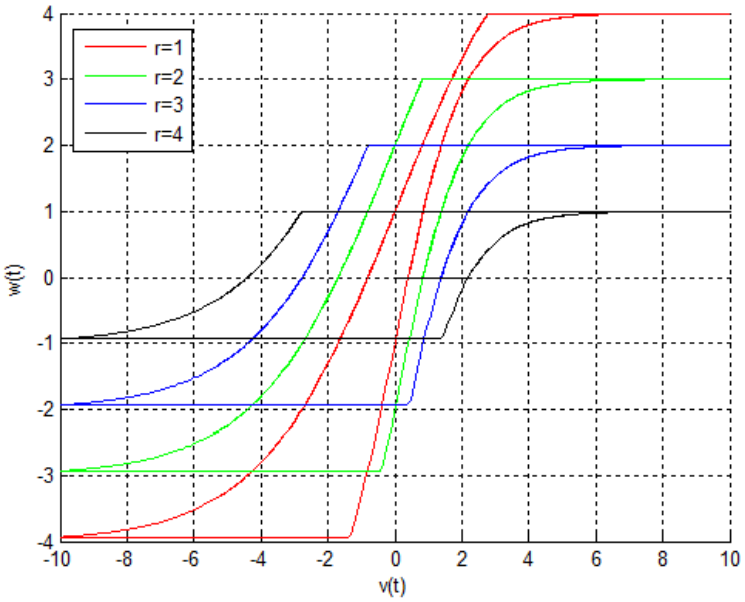

(b) generalized play operator

Figure 3.7: Input-output relationships under $v(t) = 10sin(t)$with different threshold r (a) Classical operator; (b) Generalized operator with $\gamma_l[v] = 5tanh(0.25v)$, $\gamma_r[v] = 5tanh(0.5v)$

As an illustration, Fig. 3.7 depicts the input-output relationships of the classical operator and

the asymmetric generalized play operator. In 3.7(b), the proposed generalized play operator can characterize a kind of asymmetric hysteresis behaviors.

3.3.2 Generalized Prandtl-Ishlinskii (GPI) Model

In [9], the proposed Generalized Prandtl-Ishlinskii (GPI) model is the weighted superposition of the generalized play operators. Analytically, the GPI model is defined as,

$$w(t) = \Pi_g[v](t) = H(v(t)) + \int_0^R p(r) F_{lr}^{\gamma}[v](t) dr \tag{21}$$

where H is a non-decreasing Lipschitz continuous function, $p(r)$ is the density function. Because the generalized play operator $F_{lr}^{\gamma}[v](t)$ is Lipschitz-continues, the GPI model $\Pi_g[v](t)$ is Lipschitz-continues for any given input $v(t) \in C_m[0, t_E]$. With the multiple choices of envelop functions, the GPI model can represent a more general kind of hysteresis shapes. For the same input $v(t) = tsin(2\pi t)$, Fig. 3.8 and Fig. 3.9 show the input-output properties of each model and their related element hysteresis operators.

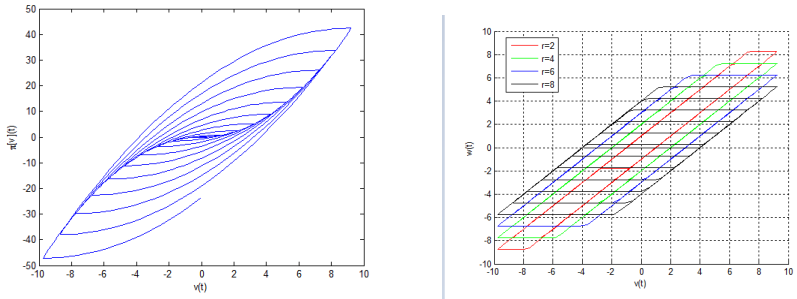

(a) hysteresis behavior (b) operator behavior

Figure 3.8: Input-output relationships under $v(t) = tsin(2\pi t)$ of classical PI model

From the diagram of the input-output relationship of the GPI model and the behavior of the generalized play operator, there are some observations of the GPI model.

(1) In the generalized play operator, the threshold of the operator is no longer r. From the initial status $w = 0$, the output of the operator keeps constant until the input signal $v(t)$ crosses $\gamma_l[v](t) - r = 0$ or $\gamma_r[v](t) + r = 0$, which makes the new threshold of the operator $\gamma_l^{-1}(r)$ and $\gamma_r^{-1}(-r)$. In this case, the threshold of the operator is also related to the envelop functions

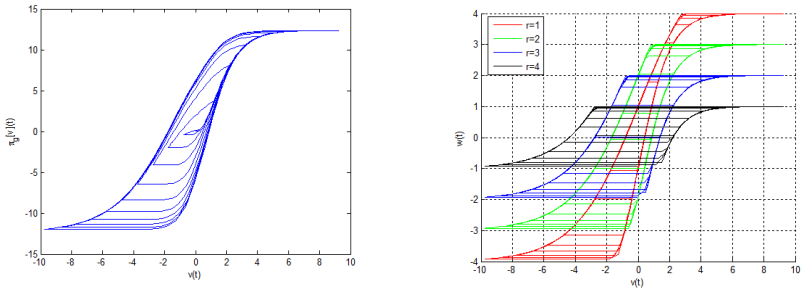

(a) Hysteresis behavior (b) Operator behavior

Figure 3.9: Input-output relationships under $v(t) = tsin(2\pi t)$ of GPI model with evnelop functions $\gamma_l[v] = 5tanh(0.25v)$ and $\gamma_r[v] = 5tanh(0.5v)$

$\gamma[v]$, which may cause different meaning in threshold.

(2) With the definition $f_{lr}^{\gamma}(v, w) = max\{\gamma_l(v) - r, min\{\gamma_r(v) + r, w\}\}$, the boundaries of the generalized play operator are the envelop functions $\gamma[v]$ translated along $y/w(t)$ axis, but not along $x/v(t)$ axis. With this property, some characters of the envelop functions will be lost. For example, in Fig. 3.7(b), the envelop functions $\gamma_l[v] = 5tanh(0.25v)$ and $\gamma_r[v] = 5tanh(0.5v)$ are bounded between ± 5 which may be useful to present a kind of saturated hysteresis. Nevertheless, with generalized play operator, this property become harder to be used, or even lost.

(3) Compared with the classical PI model, the GPI model replaced the input signals $v(t)$ with the $\gamma[v](t)$, which may be regarded as a cascade of the preprocessing function $\gamma[v]$ and the classical PI model, as Fig. 3.10.

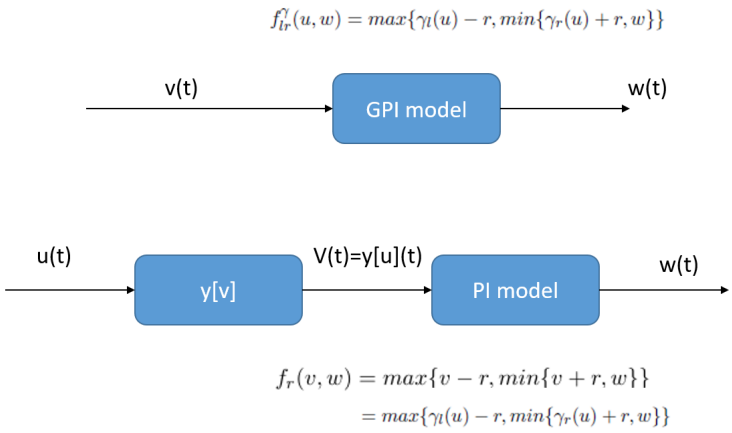

Figure 3.10: The GPI model can be regarded as the cascade of the preprocessing $\gamma[v](t)$ and the classical PI model

3.4 Modified Generalized Prandtl-Ishlinskii (mGPI) Model

With the above observations, the GPI may need to be further modified or re-defined to overcome above limits. Based on the discussions of the GPI model in the previous section, the modified Generalized Prandtl-Ishlinskii (mGPI) Model is proposed as follows.

3.4.1 Modified Generalized Play Operator

Analytically, the modified generalized play operator for any input $v(t) \in C_E[0, t_E]$ and threshold r is defined as

$$\begin{cases} F_{mr}^{\gamma}[v](0) = f_{mr}^{\gamma}(v(0), 0) = w(0) \\ F_{mr}^{\gamma}[v](t) = f_{mr}^{\gamma}(v(0), w(t_i)) \end{cases} \tag{22}$$

with

$$f_{mr}^{\gamma}(v, w) = max\{\gamma_l(v - r), min\{\gamma_r(v + r), w\}\} \tag{23}$$

for $t_i < t \leq t_{i+1}$ and $0 \leq i \leq N - 1$.

Some of the key properties of the modified generalized play operator are as follows,

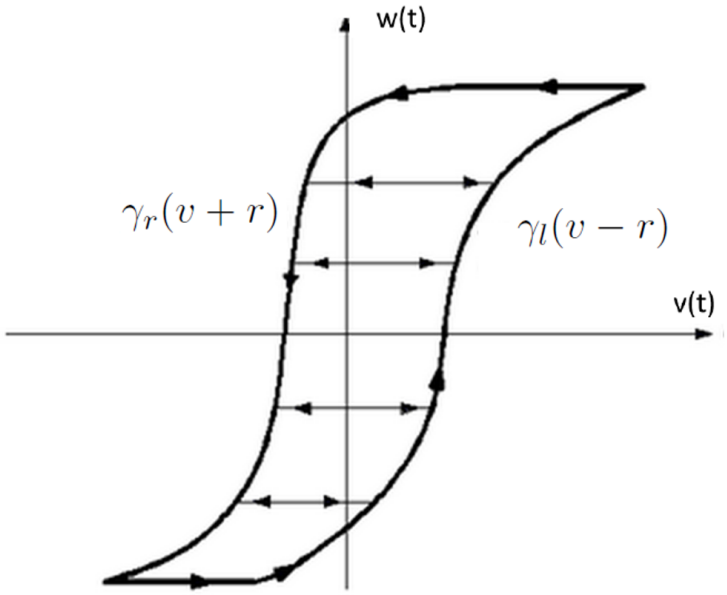

Figure 3.11: Input-output relationship of the modified generalized play operator

- Lipschitz-continuity. Like the generalized play operator [9], for a given input $v(t)$, Lipschitz-continuity of the modified generalized play operator can be ensured if the functions γ_l and γ_r are Lipschitz continuous.

- Rate-independence. The modified generalized play operator $F_{mr}^{\gamma}[v]$ is a rate-independent hysteresis operator, based on the definition in [7],

$$F_{mr}^{\gamma}[v] \circ \phi = F_{mr}^{\gamma}[v \circ \phi] \tag{24}$$

- Counter-clockwise. As Fig. 3.11 shows, the input-output trajectory of the modified generalized play operator is counter-clockwise.

As illustrated in Fig. 3.11, it is important to note that the hysteresis shape of the modified generalized play operator is bounded by the two strictly increasing envelop functions $\gamma_l(v-r)$ and $\gamma_r(v+r)$. Thus, the threshold of the modified generalized play operator are the solutions of $\gamma_l(v-r)=0$ and $\gamma_r(v+r)=0$, which are $\gamma_l^{-1}+r$ and $\gamma_r^{-1}-r$. If $\gamma(0)=0$ is chosen, the threshold of the modified generalized play operator is $\pm r$. Besides, the boundaries of the modified

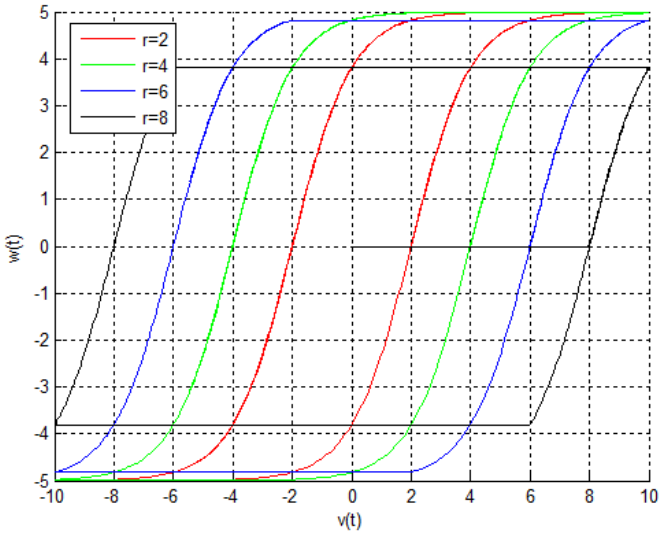

Figure 3.12: Input-ouput relationship of the modified generalized play operator with different threshold r, with $\gamma_l[v] = \gamma_r[v] = 5tanh(0.5v(t))$

generalized play operator are the envelop functions $\gamma[v]$ translated along the g $x/v(t)$ axis, keeping the same shape and boundaries of the envelop functions $\gamma[v]$. These properties makes the modified generalized play operator a potential better choice to describe hysteresis behaviors.

3.4.2 Modified Generalized Prandtl-Ishlinskii (mGPI) Model

Similar to the GPI model $\Pi_g[v](t)$, the mGPI $\Pi_m[v](t)$ model is defined as the weighted integral of the modified generalized play operator $F^{\gamma}_{mr}[v]$,

$$w(t) = \Pi_m[v](t) = p_0 F^{\gamma}_{m0}[v](t) + \int_0^R p(r) F^{\gamma}_{mr}[v](t) dr \tag{25}$$

where p_0 is a positive constant, $F^{\gamma}_{m0}[v](t)$ denotes a modified generalized play operator $F^{\gamma}_{mr}[v](t)$ with $r = 0$, $p(r)$ is the density function. The mGPI model $\Pi_m[v](t)$ is Lipschitz-continues for any given input $v(t) \in C_m[0, t_E]$, because the modified generalized play operator is Lipschitz-continues.

3.4.3 Some Examples

In this subsection, some examples of representing hysteresis nonlinearities using the proposed mGPI model are provided with different envelop functions. The input signals are $v(t) = 6sin(\pi t) + 4cos(3.3\pi t);$, $t \in [0, 10]$. For the mGPI model, $p_0 = 1$ and $p(r) = e^{-0.1r}$. Input-output relationships of the mGPI model with different envelop functions are shown in Table 3.1.

Table 3.1: Examples of the mGPI model with different envelop functions.

Fig. 3.13	$\gamma_l[v] = \gamma_r[v] = v$
Fig. 3.14	$\gamma_l[v] = \gamma_r[v] = 3v$
Fig. 3.15	$\gamma_l[v] = \gamma_r[v] = tanh(0.5v)$
Fig. 3.16	$\gamma_l[v] = 20tanh(0.1v + 0.2)$ and $\gamma_r[v] = 20tanh(0.2v + 0.1)$

In the 4 sets of envelop functions chosen, the first set of envelop functions are the identity functions $\gamma[v] = v$. In this case, the mGPI model will become the classical PI model. As shown in Fig. 3.13, the mGPI model with $\gamma[v] = v$ performs as the classical PI model. The second set of envelop functions employed are the linear functions $\gamma[v] = 3v$. As depicted in Fig. 3.14, hysteresis performs similar to the classical PI model. The third set of envelop functions used are the nonlinear functions $\gamma[v] = tanh(0.5v)$. As shown in Fig. 3.15, the mGPI model with these nonlinear envelop functions can describe a different kind of hysteresis nonlinearities. In the forth set, the asymmetric envelop functions $\gamma_l[v] = 20tanh(0.1v + 0.2)$ and $\gamma_r[v] = 20tanh(0.2v + 0.1)$ are utilized. In Fig. 3.16, the figure illustrates that the mGPI model can characterize asymmetric hysteresis nonlinearities with asymmetric envelop functions.

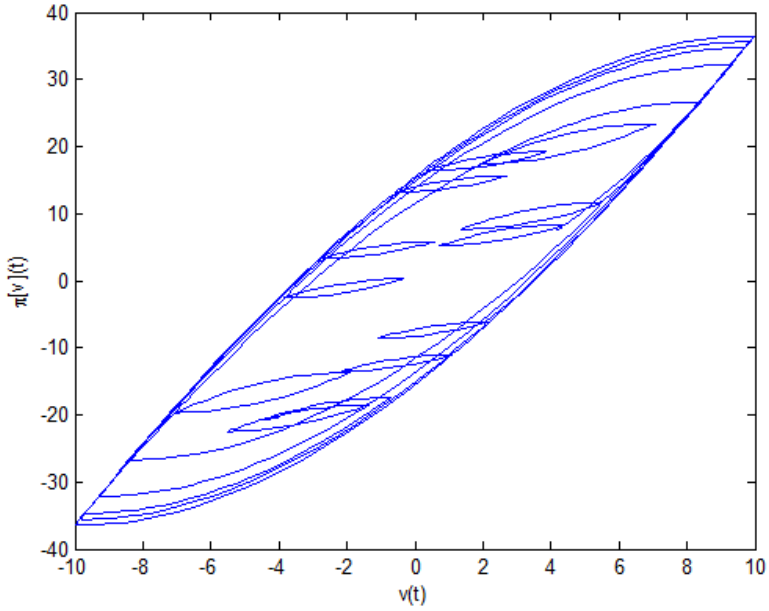

(a) modified GPI model

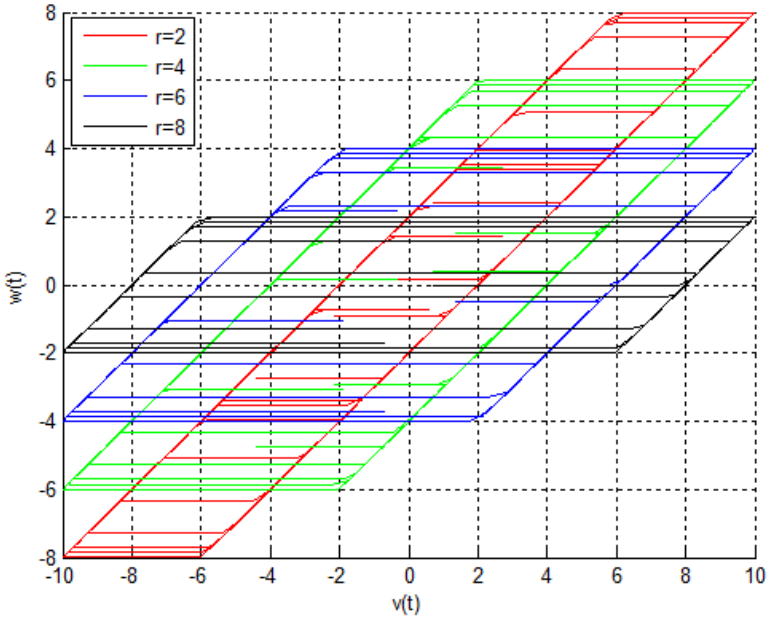

(b) modified generalized play operator

Figure 3.13: Examples with $\gamma_l[v] = \gamma_r[v] = v$

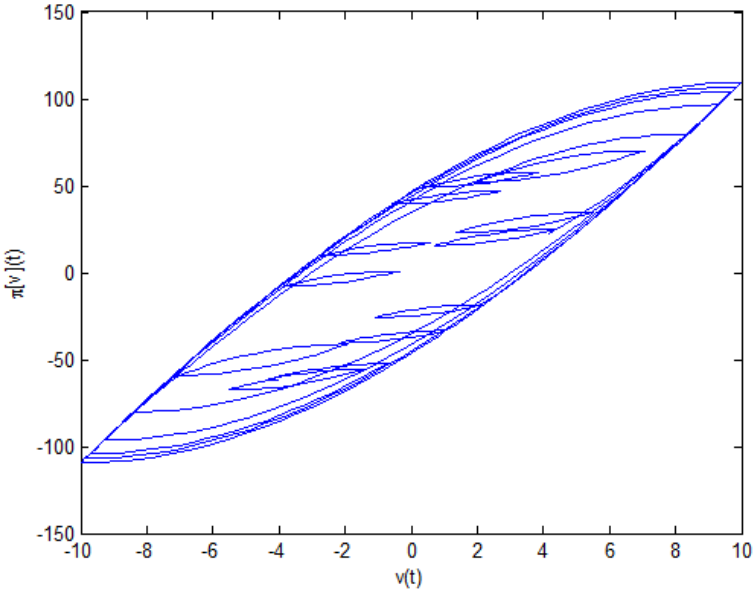

(a) modified GPI model

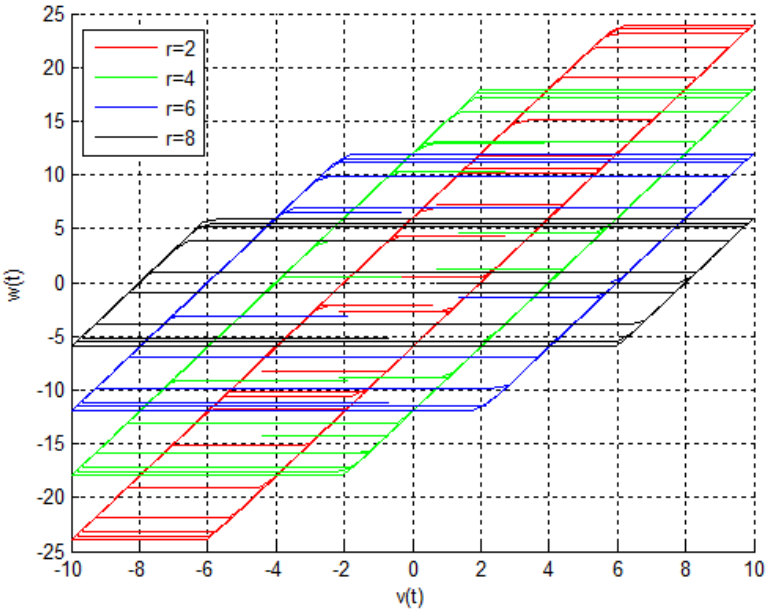

(b) modified generalized play operator

Figure 3.14: Examples with $\gamma_l[v] = \gamma_r[v] = 3v$

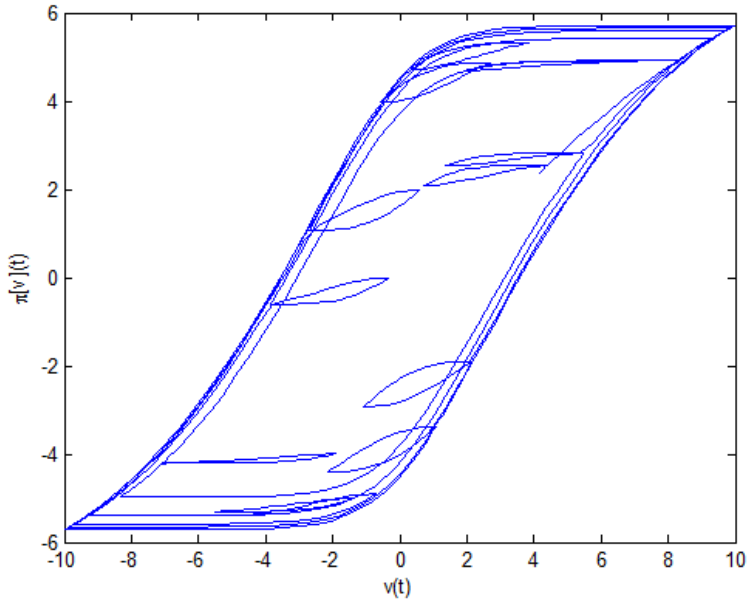

(a) modified GPI model

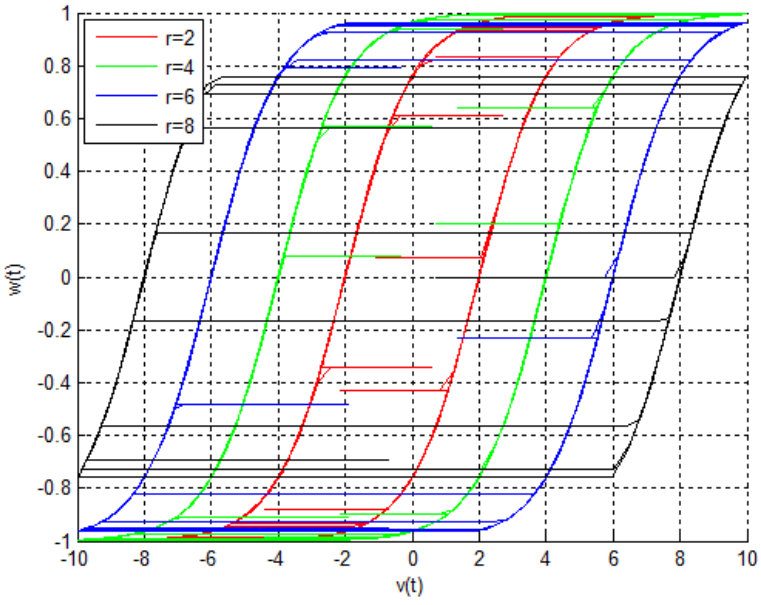

(b) modified generalized play operator

Figure 3.15: Examples with $\gamma_l[v] = \gamma_r[v] = tanh(0.5v)$

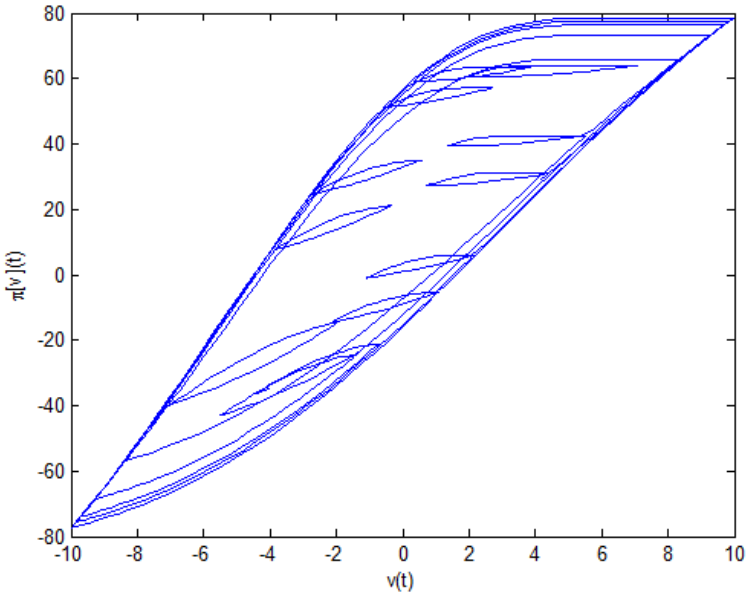

(a) modified GPI model

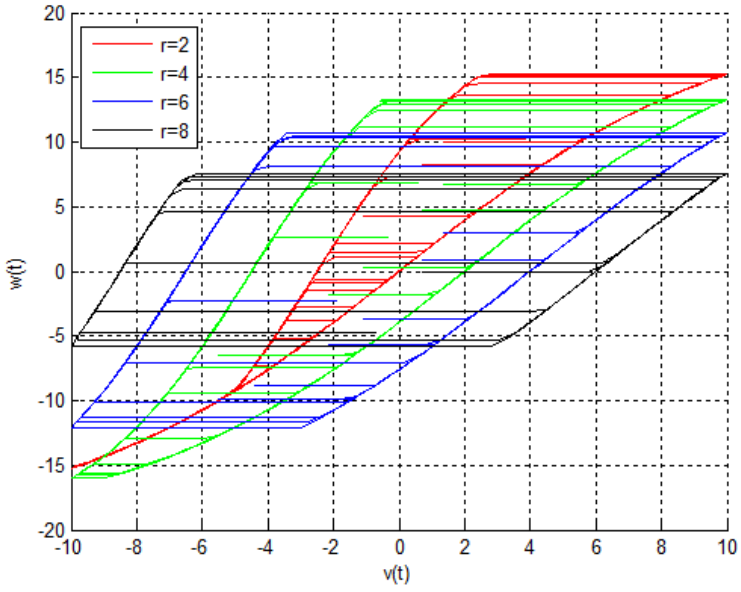

(b) modified generalized play operator

Figure 3.16: Examples with $\gamma_l[v] = 20tanh(0.1v + 0.2)$ and $\gamma_r[v] = 20tanh(0.2v + 0.1)$

3.5 Comparison of mGPI Model with classical PI model and GPI Model

In this section, the proposed mGPI model $\Pi_m[v]$ will be compared with the classical PI model $\Pi[v]$ and the available GPI model $\Pi_g[v]$. As outlined in the previous sections, these models can be written as

$$\begin{cases} \Pi[v](t) = p_0 v(t) + \int_0^R p(r) F_r[v](t) dr \\ f_r(v, w) = max\{v - r, min\{v + r, w\}\} \end{cases} \tag{26}$$

$$\begin{cases} \Pi_g[v](t) = H(v(t)) + \int_0^R p(r) F_{lr}^{\gamma}[v](t) dr \\ f_{lr}^{\gamma}(v, w) = max\{\gamma_l(v) - r, min\{\gamma_r(v) + r, w\}\} \end{cases} \tag{27}$$

$$\begin{cases} \Pi_m[v](t) = p_0 F_{m0}^{\gamma}[v](t) + \int_0^R p(r) F_{mr}^{\gamma}[v](t) dr \\ f_{mr}^{\gamma}(v, w) = max\{\gamma_l(v - r), min\{\gamma_r(v + r), w\}\} \end{cases} \tag{28}$$

To compare the differences of the models themselves, the parameters of these models are set the same. $R = 10$, $p_0 = 1$, and $p_r = e^{-0.1r}$ are selected for all the models. For the GPI model and the mGPI model, $y_l = 10tanh(0.2r)$ and $y_r = 10tanh(0.1r)$ are set as the envelop functions. All the following simulations in this section are with the input $v(t) = 10sin(2\pi t) + t$, $t \in [0, 10]$. The input-output relationships and the behaviors of the related operators are shown in Figs. 3.17 - 3.19, where only operators with $r = 2, 4, 6, 8, 10$ are illustrated and analyzed.

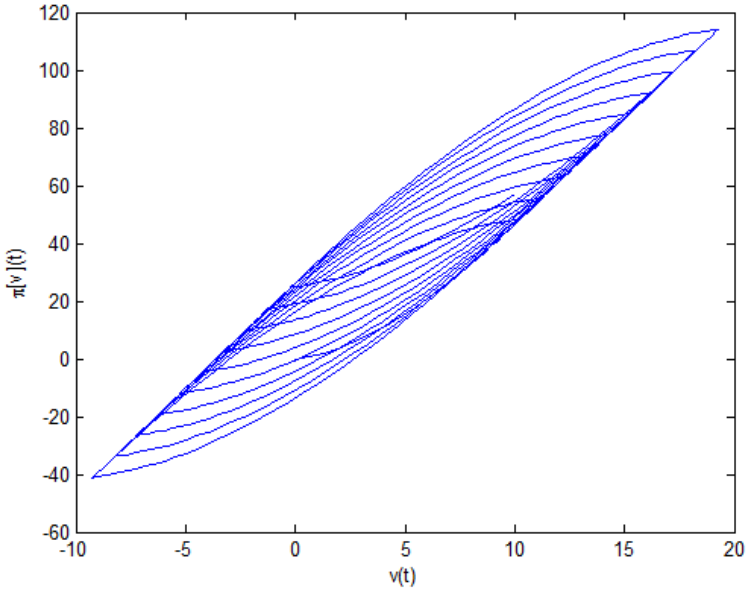

(a) Input-output relationship

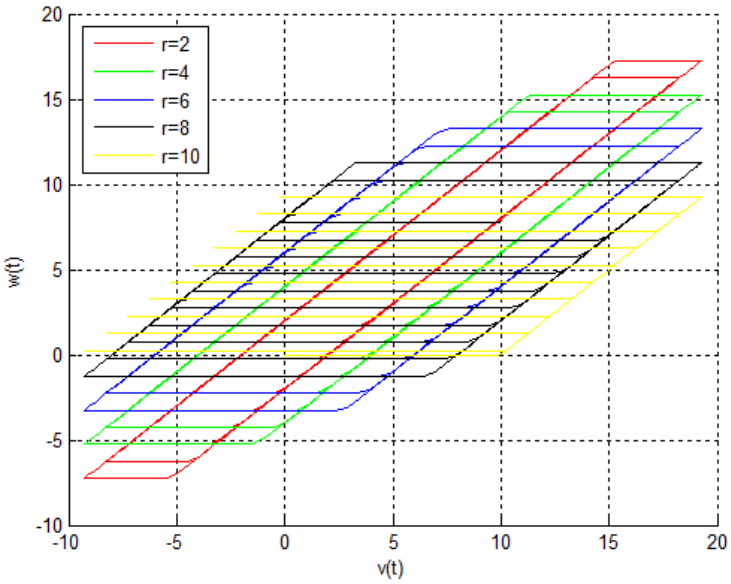

(b) Operators behaviors

Figure 3.17: PI Model

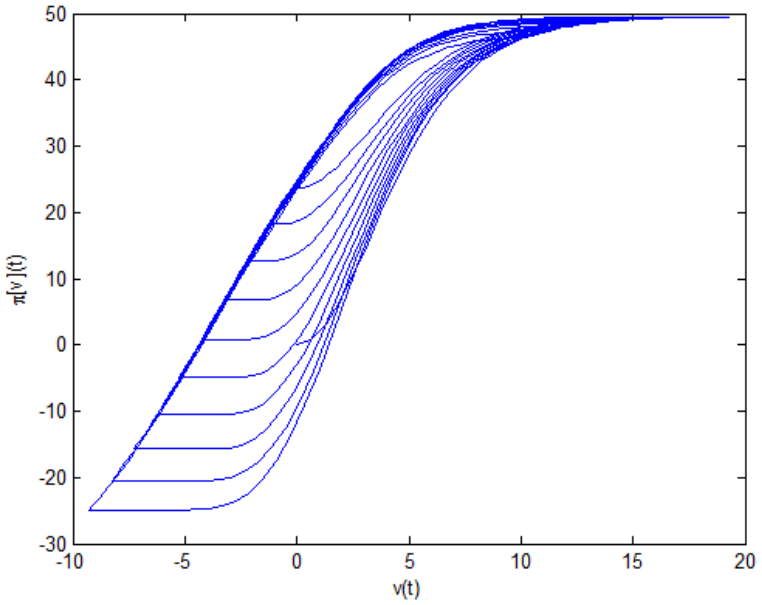

(a) Input-output relationship

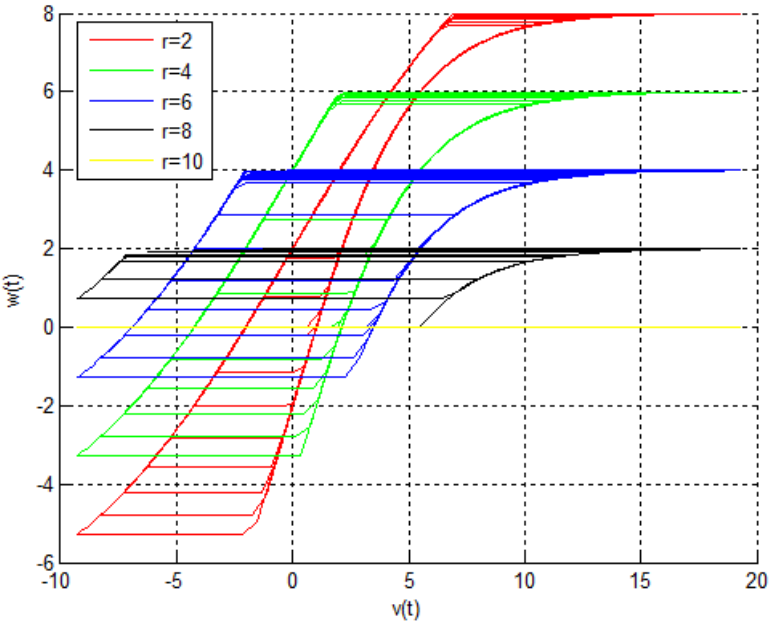

(b) Operators behaviors

Figure 3.18: GPI Model

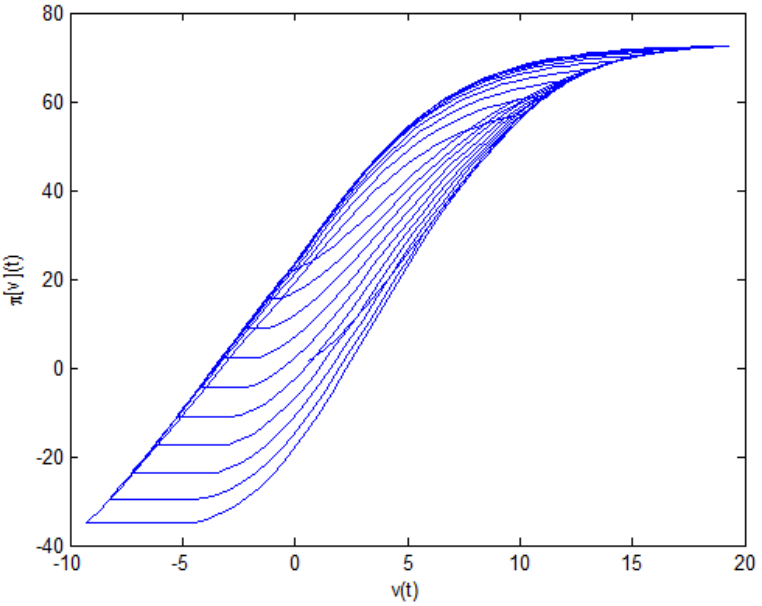

(a) Input-output relationship

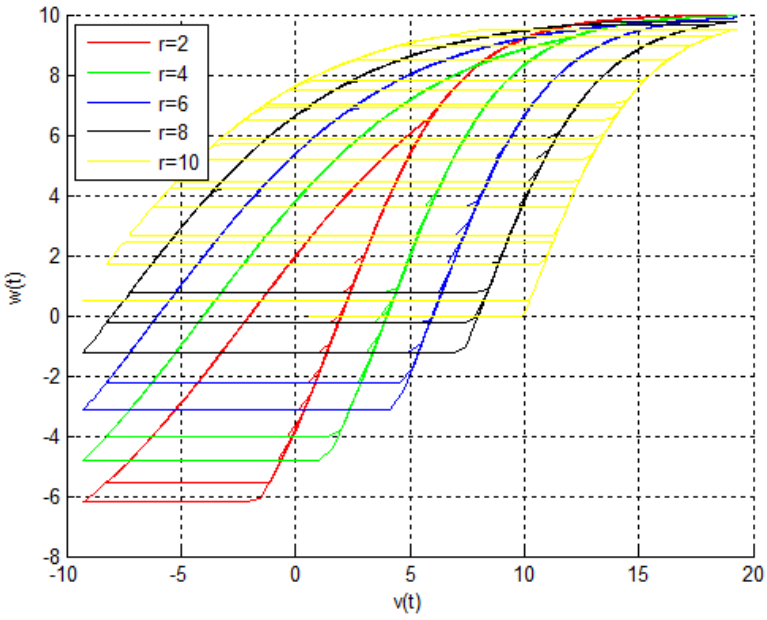

(b) Operators behaviors

Figure 3.19: mGPI Model

From these figures, some of the observations of the proposed mGPI model are discussed as follows,

(1) Both the GPI model and the proposed mGPI model can describe a kind of asymmetric hysteresis nonlinearities with $\gamma_l \neq \gamma_r$. While the classical PI model, can only describe symmetric hysteresis behaviors.

(2) As shown in Fig. 3.18(a) and Fig. 3.19(a), with the same input, same density functions, and same envelop functions, the proposed mGPI model and the available GPI model lead to two hysteresis loops with different shapes and output magnitudes, which implies the different definitions of the operators result in different descriptions of the hysteresis. It explains why the proposed mGPI model is needed.

(3) In the classical PI model, the threshold of each operator is the parameter r, as shown in the intersection points of the trajectory of the operators and the x axis in Fig. 3.17(b). However, in the GPI model, the threshold is no longer r of each operators. As discussed in Section 3.3, it is related to the envelop functions $\gamma[v]$. In the proposed mGPI model, as shown in Fig. 3.19(b), though the boundaries of the operators are asymmetric curves, the threshold of each operator is still $\pm r$. It can be said that the mGPI model keeps the original meaning of the threshold r.

(4) To characterize the saturated hysteresis nonlinearities, the bounded envelop functions $\gamma[v]$ are employed. For example, $y_l = 10tanh(0.2r)$ and $y_r = 10tanh(0.1r)$, which are bounded between ± 10, are applied in the simulations in this section. In the GPI model, the boundaries of the generalized play operator are the envelop functions $\gamma[v]$ translated along $y/w(t)$ axis. Thus, the bounds of the operators vary with different r. In the mGPI model, the boundaries of the operators are the envelop functions $\gamma[v]$ translated along $x/v(t)$ axis. As shown in Fig. 3.19(b), the upper bounds of all the operators ar 10. In this case, the upper bound of the hysteresis output can be easily calculated as

$$Q = U * (p_0 + \int_0^R p(r)) \tag{29}$$

where $U = 10$ is the upper bound of the modified generalized play operator. Since $R = 10$, $p_0 = 1$, and $p_r = e^{-0.1r}$ are used in this section, the upper bound of the output of the mGPI

model can be easily calculated as $10(1+10-10e^{-1}) \approx 73.2$, which is the same as shown in Fig.3.19(a). In the GPI model, due to the bounds of the operators vary, the bounds of the hysteresis output can not be determined easily, leading to the difficulty for the description of the required bounds.

(5) In Fig. 3.18(b), the behavior of the generalized play operator with $r = 10$, which is shown in the yellow line, keeps constant zero. Because the right (lower) boundary of the operator is $10tanh(0.2r) - 10 < 0$ and the left (upper) boundary $10tanh(0.1r) + 10 > 0$ for any input r, this operator will not function any more. This issue is alleviated because the density function $p(r)$ generally chosen as an exponential function with minus r. Thus, for a large r, $p(r)$, which is multiplied with the operators, becomes small enough to be ignored. However, in a good hysteresis model, the operator should always work.

3.6 Summary

In this chapter, the classical Prandtl-Ishlinskii (PI) model and the Generalized Prandtl-Ishlinskii (GPI) model are reviewed. Subsequently, a modified Generalized Prandtl-Ishlinskii (mGPI) model is proposed. Several simulations are demonstrated to validate the effectiveness of the proposed model and its related modified generalized play operator.

Compared with the GPI model, the proposed mGPI model is with following advantages in describing the hysteresis nonlinearities.

(1) The threshold of the proposed modified generalized play operator is $\pm r$, if the envelop functions γ_l and γ_r satisfying $\gamma(0) = 0$, while the new thresholds of the generalized play operator are $\gamma_l^{-1}(r)$ and $\gamma_r^{-1}(-r)$. In this case, threshold of the proposed operator is independent from the envelop functions, which keeps the initial definition and the property of the threshold $\pm r$. Therefore, other research results about the element hysteresis operator can be applied to the proposed modified generalized play operator easier.

(2) Different from the generalized play operator, the boundaries of the modified generalized play operator are the envelop functions $\gamma[v]$ translated along $x/v(t)$ axis, but not along $y/w(t)$

axis. Consequently, properties of the envelop functions will not be lost. For example, in Fig. 3.15, the envelop functions $\gamma[v] = tanh(0.5v)$ is bounded between ± 5, which is inherited by the modified generalized play operator. This may be useful to present a kind of saturated hysteresis.

(3) The mGPI model is not a directly cascade of the classical PI model with the preprocessing part $\gamma[v](t)$, which can be useful in describing a more complicated hysteresis.

Chapter 4

Analytical Inverse of the Modified Generalized Prandtl-Ishlinskii (mGPI) Model

The controller development for systems with hysteresis nonlinearities is challenging, because the hysteresis effect usually worsen control performances, lead oscillations or even instabilities. One popular strategy for hysteresis controller designs is the inverse-model-based control method, which is depicted in Subsection 2.3.1. Unlike the Preisach model and the KP model, the PI model is analytical invertible, which is useful in inverse compensation [8].

However, according to the definition, the PI model can only describe a class of symmetric and non-saturated hysteresis, recent researches focused on generalizing the PI model, making it able to describe a more complicated kind of hysteresis, while keeping invertibility property. In Section 3.3, a Generalized PrandtlIshlinskii (GPI) model from the literature [9] was introduced, whose analytical inverse has been provided in [10]. To overcome the the limitations of the GPI model, in Section 3.4, a modified Generalized Prandtl-Ishlinskii (mGPI) model was proposed.

In this chapter, an analytical inverse of the proposed modified Generalized Prandtl-Ishlinskii (mGPI) model will be derived, which can be used as an inverse compensator of the hysteresis nonlinearities. Subsequently, the numerical implementation method of the proposed inverse model

will be provided.

4.1 Initial Loading Curve

In [7], the inverse of the classical PI model is derived with the help of the initial loading curve. The initial loading curve is used as alternative description of the Prandtl-Ishlinskii model. It is an essential tool for the derivation of the inverse of the proposed mGPI model. Consequently, it is necessary to introduce the initial loading curve.

4.1.1 Initial Loading Curve for Classical PI model

The initial loading curve refers to an input-output relation, generated by the input increasing from zero to the final value. For the PI model, the initial loading curve can be represented by,

$$\phi(r) = p_0 r + \int_0^r p(\theta)(r-\theta)d\theta \tag{30}$$

The density functions $p(r)$ and the constant p_0 can be derived from the initial loading curve as,

$$p_0 = \phi'(0) \tag{31}$$

and

$$p(r) = \phi''(r) \tag{32}$$

Thus, the PI model can be presented using initial loading curve as parameters as follows,

$$\begin{aligned} w(t) = \Pi[v](t) &= p_0 v(t) + \int_0^R p(r) F_r[v](t) dr \\ &= \phi'(0) v(t) + \int_0^R \phi''(r) F_r[v](t) dr \end{aligned} \tag{33}$$

As an example, a hysteresis represented by PI model is as follows,

$$w(t) = \Pi[v](t) = 1 \times v(t) + \int_0^R e^{-0.1r} F_r[v](t) dr \tag{34}$$

whose input-output relation is shown in Fig. 4.1. According to the definition of the initial loading curve of the classical PI model, the loading curve of (34) is,

$$\begin{aligned}\phi(r) &= \int_0^r p_0 dr + \int_0^r p(\theta)(r-\theta)d\theta \\ &= 1 \times r + \int_0^r e^{-0.1\theta}(r-\theta)d\theta \\ &= r + 10r - 100 + 100e^{-0.1r} \\ &= 11r - 100 + 100e^{-0.1r}\end{aligned} \tag{35}$$

As a validation, the initial loading curve from simulation result and the derived loading curve are shown in Fig. 4.2. It can be observed that these two curves are the same.

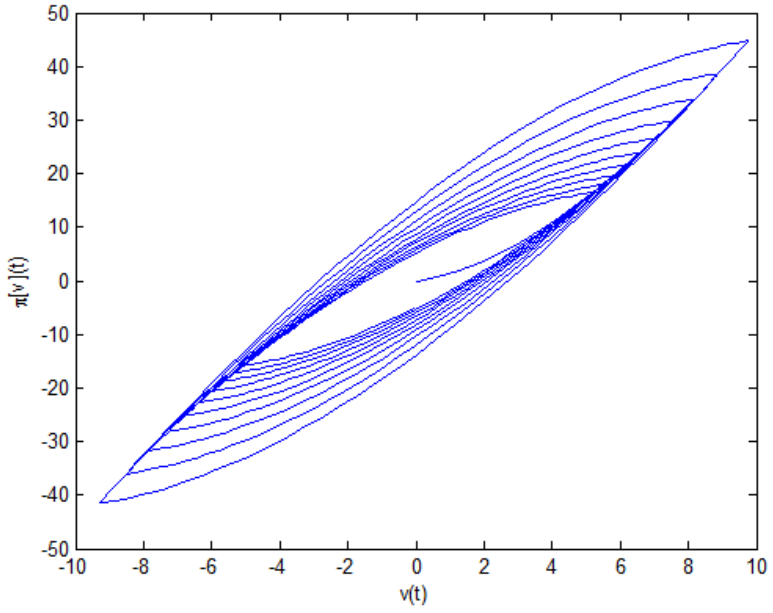

Figure 4.1: input-output relation of (34) with $v(t) = 10sin(2\pi t)/(1+0.1t)$, $t \in [0, 10]$

4.1.2 Initial Loading Curve for mGPI Model

Similar to the initial loading curve of the classical PI model (30), concerning the mGPI model

$$w(t) = \Pi_m[v](t) = p_0 F^{\gamma}_{m0}[v](t) + \int_0^R p(r) F^{\gamma}_{mr}[v](t) dr \tag{36}$$

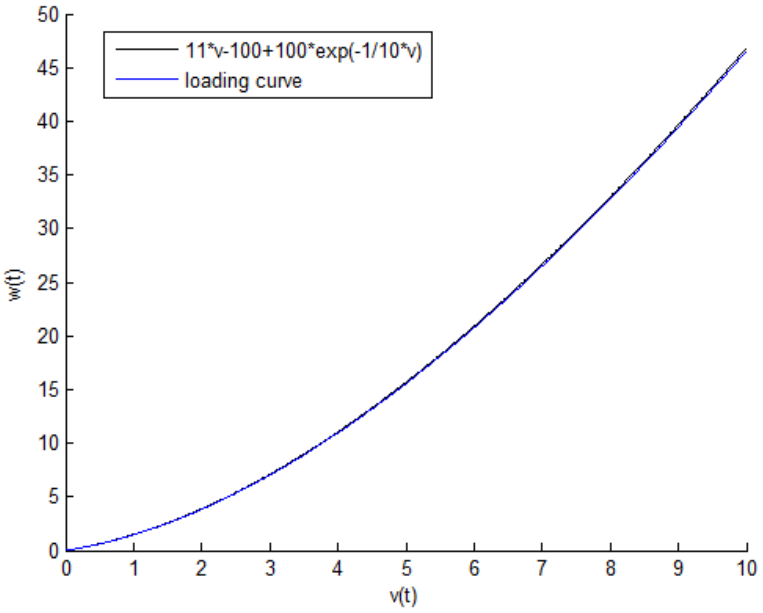

Figure 4.2: The simulated and the derived loading curve

The loading curve of the mGPI model can be expressed as,

$$\phi(r) = p_0\gamma(r) + \int_0^r p(\theta)\gamma(r-\theta)d\theta \tag{37}$$

It can be observed that when the envelop function $\gamma[v]$ is chosen the linear function $\gamma[v] = v$, the loading curve of the mGPI model (37) transform into (30), since the mGPI model become the classical PI model.

Theorem 1 (Leibniz Integral Rule) *Let $f(x,t)$ be a function such that the partial derivative of f with respect to t exists, and is continuous. Then,*

$$\frac{d}{dt}\left(\int_{a(t)}^{b(t)} f(x,t)dx\right) = \int_{a(t)}^{b(t)} \frac{\partial f}{\partial t}dx + f\left(b(t),t\right)\cdot b'(t) - f\left(a(t),t\right)\cdot a'(t) \tag{38}$$

With the Theorem 1, the derivative of the loading curve of the mGPI model (37) can be expressed as,

$$\phi'(r) = p_0\gamma'(r) + \int_0^r p(\theta)\gamma'(r-\theta)d\theta + p(r)\gamma(0) \tag{39}$$

If $\gamma(0) = 0$ is chosen for the envelop functions, the derivative of the loading curve (39) can be written as,

$$\phi'(r) = p_0\gamma'(r) + \int_0^r p(\theta)\gamma'(r-\theta)d\theta \tag{40}$$

4.2 Analytical Inverse of the modified Generalized Prandtl-Ishlinskii (mGPI) Model

In [7], the inverse of the classical PI model is provided, based on the strategy that the initial loading curve of the hysteresis model ϕ and the loading curve of the inverse model ψ are skew symmetry, following

$$\psi \circ \phi(r) = r \tag{41}$$

Similar to the derivation of the inverse classical PI model, because the mGPI model and its inverse share similar properties, the analytical inverse can be written as another mGPI model as,

$$w(t) = \Pi_m^{-1}[v](t) = g_0 F_{m0}^{\beta}[v](t) + \int_0^Q g(q)F_{mq}^{\beta}[v](t)dq \tag{42}$$

where g_0 is a positive constant, $g(r)$ is the density functions, β is the envelop function, $F_{mr}^{\beta}[v]$ is a modified generalized play operator with threshold q and envelop function β.

Thus, the loading curve of the inverse mGPI model is

$$\psi(q) = g_0\beta(q) + \int_0^q p(\eta)\beta(r-\eta)d\eta \tag{43}$$

and its derivative

$$\psi'(q) = g_0\beta'(q) + \int_0^q p(\eta)\beta'(q-\eta)d\eta \tag{44}$$

Substitute the derivatives of these two loading curves into (41), it can be derived that,

$$g_0 = p_0^{-1} \tag{45}$$

and

$$\beta[v] = \gamma^{-1}[v] \tag{46}$$

Therefore, the inverse of the mGPI model can be written as,

$$w(t) = \Pi_m^{-1}[v](t) = p_0^{-1} F_{m0}^{\gamma^{-1}}[v](t) + \int_0^Q g(q) F_{mq}^{\gamma^{-1}}[v](t) dq \tag{47}$$

The last thing remaining is the density function $g(q)$. With (41), $g(q)$ can be obtained as,

$$\int_0^q g(\eta)(\gamma^{-1})'(q-\eta)d\eta = \frac{1}{p_0\gamma'(r) + \int_0^r p(\theta)\gamma'(r-\theta)d\theta} - \frac{1}{p_0}(\gamma^{-1})'(q) \tag{48}$$

4.3 Numerical Implementation of the Inverse of the modified Generalized Prandtl-Ishlinskii (mGPI) Model

In practice, the hysteresis nonlinearities can approximately be described by a small number of element hysteresis operators [32]. Therefore, the numerical expression of the mGPI model can be written as

$$\begin{aligned} w(t) = \Pi_m[v](t) &= p_0 F_{m0}^{\gamma}[v](t) + \int_0^R p(r) F_{mr}^{\gamma}[v](t) dr \\ &= p_0 F_{m0}^{\gamma}[v](t) + \sum_{i=1}^{N} p(r_i) F_{mr_i}^{\gamma}[v](t) \end{aligned} \tag{49}$$

where N is the number of the modified generalized play operators, r_i is the threshold r of the i_{th} operator, satisfying $0 = r_0 < r_1 < \cdots < r_N = R$. and the proposed inverse mGPI model can be written as,

$$
\begin{aligned}
w(t) = \Pi_m^{-1}[v](t) &= g_0 F_{m0}^{\beta}[v](t) + \int_0^Q g(q) F_{mq}^{\beta}[v](t) dq \\
&= g_0 F_{m0}^{\beta}[v](t) + \sum_{i=1}^{N} g(q_i) F_{mq_i}^{\beta}[v](t)
\end{aligned}
\tag{50}
$$

where N is the number of the modified generalized play operators, q_i is the threshold q of the i_{th} operator, satisfying $0 = q_0 < q_1 < \cdots < q_N = Q$.

Parameters required calculation in the inverse model are g_0, $\beta[v]$, q_i, and $g(q_i)$.

Thus, the initial loading curve of the mGPI model and its inverse for $r \in [r_j, r_{j+1})$ and $q \in [q_j, q_{j+1})$ can be written as,

$$
\begin{cases}
\phi(r_j) = p_0 \gamma(r_j) + \sum_{i=1}^{j} p(r_i) \gamma(r_j - r_i) \\
\psi(q_j) = g_0 \beta(q_j) + \sum_{i=1}^{j} g(q_i) \beta(q_j - q_i)
\end{cases}
\tag{51}
$$

The derivatives of the loading curves for $r \in [r_j, r_{j+1})$ and $q \in [q_j, q_{j+1})$ are as follows

$$
\begin{cases}
\phi'(r) = p_0 \gamma'(r_j) + \sum_{i=1}^{j} p(r_i) \gamma'(r_j - r_i) \\
\psi'(q) = g_0 \beta'(q_j) + \sum_{i=1}^{j} g(q_i) \beta'(q_j - q_i)
\end{cases}
\tag{52}
$$

Because of (41), it is obvious that

$$
\psi'(q) = \frac{1}{\phi'(r)} \tag{53}
$$

Thus

$$
g_0 = \frac{1}{p_0} \tag{54}
$$

and

$$
\beta[v] = \gamma^{-1}[v] \tag{55}
$$

The results are the same as in the previous section. Because of (51), the threshold for each operator in the inverse mGPI model is,

$$q_j = p_0\gamma(r_j) + \sum_{i=1}^{j} p(r_i)\gamma(r_j - r_i) \tag{56}$$

Use (41) again,

$$\begin{aligned} \frac{1}{p_0\gamma'(r_j) + \sum_{i=1}^{j} p_i(r_j - r_i)} &= g_0\beta'(q_j) + \sum_{i=1}^{j} g_i\beta'(q_j - q_i) \\ &= g_0\beta'(q_j) + \sum_{i=1}^{j-1} g_i\beta'(q_j - q_i) + q_j\beta'(0) \end{aligned} \tag{57}$$

the density function $g(q_j)$ of the inverse mGPI model is,

$$g(q_j) = \frac{\frac{1}{\sum_{i=0}^{j}(p_i\gamma'(r_j - r_i))} - g_0\beta'(q_j) - \sum_{i=1}^{j-1} g_i\beta'(q_j - q_i)}{\beta'(0)} \tag{58}$$

Therefore, with a given mGPI model, its inverse $\Pi_m^{-1}[v] = g_0 F_{m0}^{\beta}[v] + \sum_{i=1}^{N} g(q_i) F_{mq_i}^{\beta}[v]$ can be numerical implement by following the above steps.

4.4 Summary

In this chapter, the concept of the initial loading curve is firstly introduced, which is essential for the derivation of the inverse model. Subsequently, based on the property that the initial loading curves of a model and its inverse model are skew symmetry $\psi \circ \phi(r) = r$. The analytical inverse of the mGPI model is derived. The numerical implementation methods of the proposed inverse model is provided. Following these steps, an inverse compensator of the mGPI model can be constructed.

Chapter 5

Feed-forward Compensation and Simulation Verifications

To validate the proposed mGPI hysteresis model and its inverse compensator, simulation studies will be provided in this chapter. The effectiveness of this model and the compensator is demonstrated through several simulation examples.

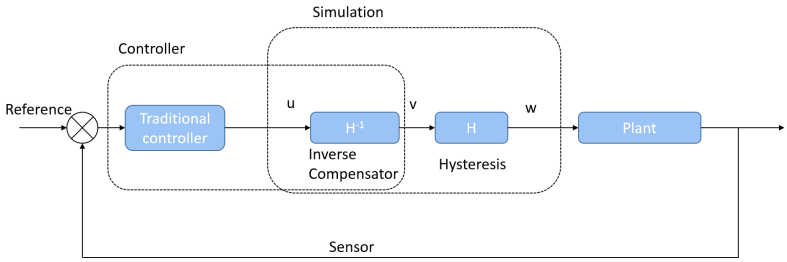

Figure 5.1: Inverse Controller Structure

Fig. 5.1 depicts a controller structure for the inverse-model-based control strategies to compensate the hysteresis. The proposed inverse of the mGPI model will be used as the inverse compensator H^{-1} in the strategy. With the use of the compensator it is expected that the signal to the plants $w(t)$ is the same as the signal from the traditional controller $u(t)$, which implies the tradition developed control methods can be directly applied.

In all the simulations in this chapter, the hysteresis nonlinearities will be described by the proposed mGPI model in Section 3.4,

$$w(t) = \Pi_m[v](t) = p_0 F^{\gamma}_{m0}[v](t) + \int_0^R p(r) F^{\gamma}_{mr}[v](t) dr \tag{59}$$

where $F^{\gamma}_{mr}[v]$ is the proposed modified generalized play operator,

$$\begin{cases} F^{\gamma}_{mr}[v](0) = f^{\gamma}_{mr}(v(0), 0) = w(0) \\ F^{\gamma}_{mr}[v](t) = f^{\gamma}_{mr}(v(0), w(t_i)) \end{cases} \tag{60}$$

with

$$f^{\gamma}_{mr}(v, w) = max\{\gamma_l(v - r), min\{\gamma_r(v + r), w\}\} \tag{61}$$

where p_0 is a positive constant, $F^{\gamma}_{m0}[v](t)$ denotes a modified generalized play operator $F^{\gamma}_{mr}[v](t)$ with $r = 0$, $p(r)$ is the density function. The selection of the density function has no standard yet. In this chapter, $p_0 = 1$ and $p(r) = e^{-0.1r}$ are selected for all the models.

For the inverse feed-forward compensator, the inverse mGPI model proposed in Section 4.2 is applied.

$$w(t) = \Pi^{-1}_m[v](t) = g_0 F^{\beta}_{m0}[v](t) + \int_0^Q g(q) F^{\beta}_{mq}[v](t) dq \tag{62}$$

where g_0 is a positive constant, $g(r)$ is the density functions, β is the envelop function, $F^{\beta}_{mr}[v]$ is a modified generalized play operator with threshold q and envelop function β.

5.1 Simulation Environment

To validate the effectiveness of the proposed model and its inverse, simulation studies using the inverse as the feed-forward compensator are provided. As shown in Fig. 5.2, a simulation platform has been established. There is a source producing the control signal $u(t)$. On the right side, the input signal $v(t)$ will be passed into the proposed mGPI model (model_MGPI block), generating output signal $w(t) = \Pi_m[v](t)$. In order to cancel the hysteresis nonlinearities, an inverse compensator (model_IMGPI block) is placed before the hysteresis block as an inverse feed-forward compensator, which means $v(t) = \Pi^{-1}_m[u](t)$, where Π^{-1}_m denotes the hysteresis inverse in (62). Thus, the output

of the hysteresis model will be $w(t) = \Pi_m[v](t) = \Pi_m \circ \Pi_m^{-1}[u](t)$. Therefore, with a precise inverse model of the hysteresis, the inverse model should compensate the hysteresis nonlinearities effectively.

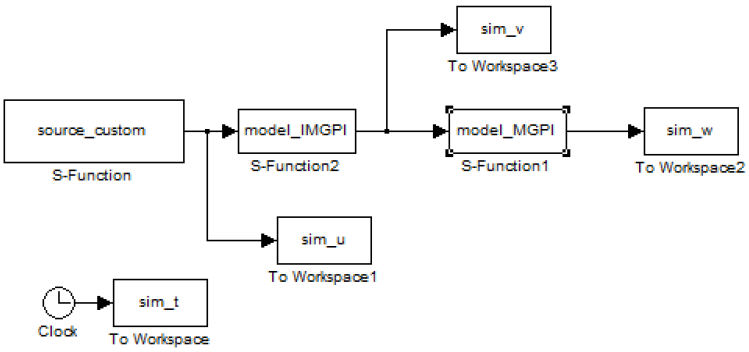

Figure 5.2: Simulation Block Diagram

In order to implement the proposed mGPI model and the inverse mGPI model, the numerical implementation methods in Section 4.3 will be utilized. Thus, the discrete form of the mGPI model can be represented as

$$\begin{aligned} w(t) = \Pi_m[v](t) &= p_0 F_{m0}^{\gamma}[v](t) + \int_0^R p(r) F_{mr}^{\gamma}[v](t) dr \\ &= p_0 F_{m0}^{\gamma}[v](t) + \sum_{i=1}^{N} p(r_i) F_{mr_i}^{\gamma}[v](t) \end{aligned} \tag{63}$$

where N is the number of the modified generalized play operators, r_i is the threshold r of the i_{th} operator, satisfying $0 = r_0 < r_1 < \cdots < r_N = R$.

In the implementation of the mGPI model. N is set as 20 in this simulation. It should be noted that the accuracy of the hysteresis model description depends on the number of N. Generally, it is unnecessary to chose a very large value. However, the selection of N should be comprised with the required accuracy and computation complexity. $r_i = 0.5i$ is chosen to make the upper limit of the integration of the mGPI model $R = r_{20} = 10$, which is large enough. p_0 is set 1. $p(r_i) = e^{-0.1r_i}(r_i - r_{i-1}) = 0.5e^{-0.1r_i}$ is set as the weight of each operator. The envelop functions

$\gamma[v]$ will be adjusted to describe different kinds of hysteresis behaviors.

The discrete form of theproposed inverse mGPI model can be written as,

$$\begin{aligned} w(t) = \Pi_m^{-1}[v](t) &= g_0 F_{m0}^{\beta}[v](t) + \int_0^Q g(q) F_{mq}^{\beta}[v](t) dq \\ &= g_0 F_{m0}^{\beta}[v](t) + \sum_{i=1}^{N} g(q_i) F_{mq_i}^{\beta}[v](t) \end{aligned} \tag{64}$$

where N is the number of the modified generalized play operators, q_i is the threshold q of the i_{th} operator, satisfying $0 = q_0 < q_1 < \cdots < q_N = Q$.

In the simulation, the number of the operators in the inverse model $N = 20$. The other parameters, including g_0, $\beta[v]$, q_i, and $g(q_i)$, will be calculated with the methods outlined in Section 4.3.

In this chapter, all the simulations are using the ode 45 solver with max step size $\Delta t = 0.01s$, under simulink of Matlab 7.6.0.

5.2 Simulation Results with Identity Function

In this section, the envelop functions are chosen the identity function $\gamma[v](t) = v(t)$. With this choice, as illustrated in Section 3.4, the proposed mGPI model will become the classical PI model. Simulations in this section will verify that the mGPI model and the inverse model can work as the classical PI model and its inverse compensator.

In this section, the input signals is chosen $u(t) = 5sin(2\pi t)/(1 + 0.1t)$, $t \in [0, 10]$. The thresholds of the 20 operators are chosen $r_i = 0.25i$. According to the inverse numerical implementation in Section 4.3, the thresholds of the 20 operators in the inverse is q_i={0.2500, 0.5610, 0.9314, 1.3598, 1.8447, 2.3848, 2.9787, 3.6251, 4.3226, 5.0700, 5.8661, 6.7097, 7.5996, 8.5347, 9.5138, 10.5358, 11.5997, 12.7045, 13.8492, 15.0327}. The Density of the 20 operators in the inverse compensator is $g(q_i)$ ={-0.1960, -0.1290, -0.0914, -0.0681, -0.0526, -0.0419, -0.0342, -0.0284, -0.0239, -0.0205, -0.0177, -0.0154, -0.0136, -0.0120, -0.0107, -0.0096, -0.0087, -0.0079, -0.0072, -0.0066}.

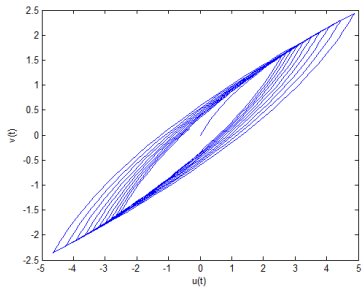

(a) Inverse Compensator

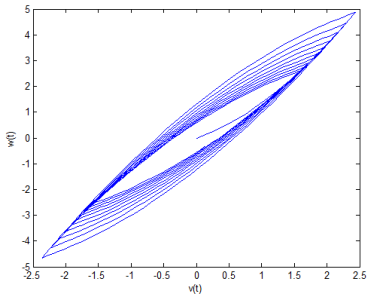

(b) Hysteresis Model

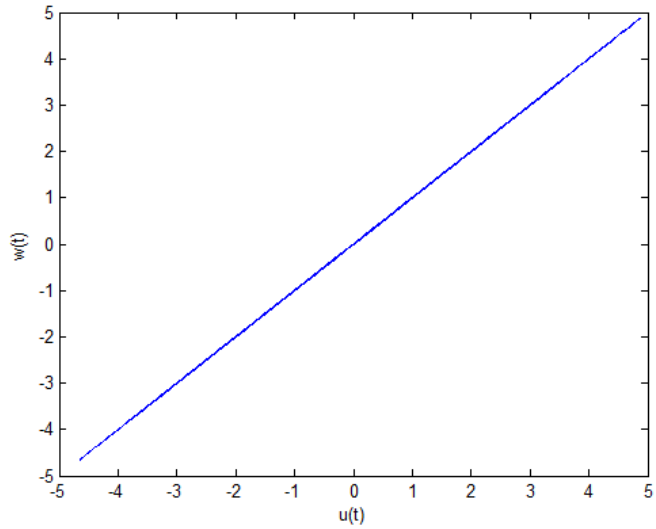

(c) Input-Output Relations with Inverse Compensation

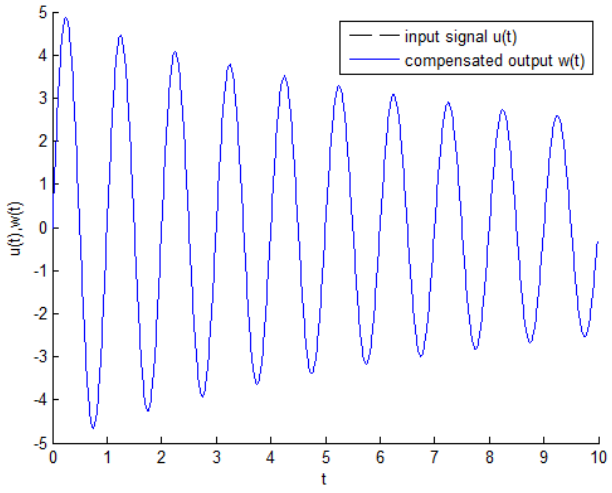

(d) $w(t)$ tracking $u(t)$

Figure 5.3: Simulation Results with $\gamma[v] = v$, and $u(t) = 5sin(2\pi t)/(1 + 0.1t)$

5.3 Simulation Results with Linear Function

In this section, the envelop functions are chosen the an linear function $\gamma[v](t) = 3v(t)$. Thus, the related functions for the inverse compensation are $\gamma'[v](t) = 3$, $\beta[v](t) = \gamma^{-1}[v](t) = \frac{1}{3}[v](t)$, and $\beta'[v](t) = \frac{1}{3}$. Simulations in this section will verify that the mGPI model and the inverse model can characterize and compensate such hysteresis.

In this section, the input signals is chosen $u(t) = 5sin(2\pi t)/(1 + 0.1t)$, $t \in [0, 10]$. The thresholds of the 20 operators are chosen $r_i = 0.25i$. According to the inverse numerical implementation in Section 4.3, the thresholds of the 20 operators in the inverse is q_i={0.7500, 1.6829, 2.7941, 4.0793, 5.5341, 7.1544, 8.9361, 10.8752, 12.9678, 15.2101, 17.5984, 20.1292, 22.7989, 25.6040, 28.5413, 31.6074, 34.7992, 38.1136, 41.5476, 45.0982}. The Density of the 20 operators in the inverse compensator is $g(q_i)$ ={-0.1960, -0.1290, -0.0914, -0.0681, -0.0526, -0.0419, -0.0342, -0.0284, -0.0239, -0.0205, -0.0177, -0.0154, -0.0136, -0.0120, -0.0107, -0.0096, -0.0087, -0.0079, -0.0072, -0.0066}. As illustrated in Fig. 5.4, with the new envelop functions, the inverse compensator translate the control signal $u(t)$ to signal $v(t)$ with amplitude of around 1.2, the hysteresis subsequently restore the signal to $w(t)$ with an amplitude of 5. The inverse compensator successfully cancel the nonlinear effect caused by hysteresis.

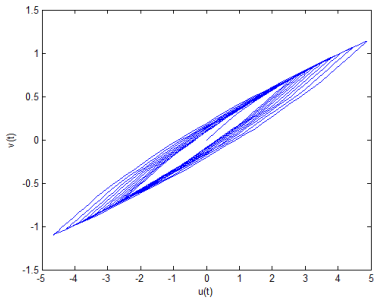

(a) Inverse Compensator

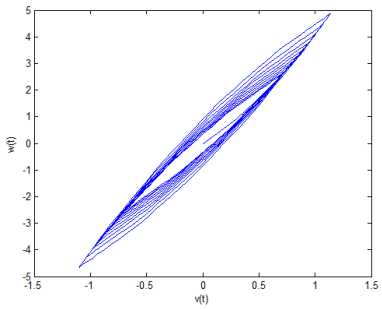

(b) Hysteresis Model

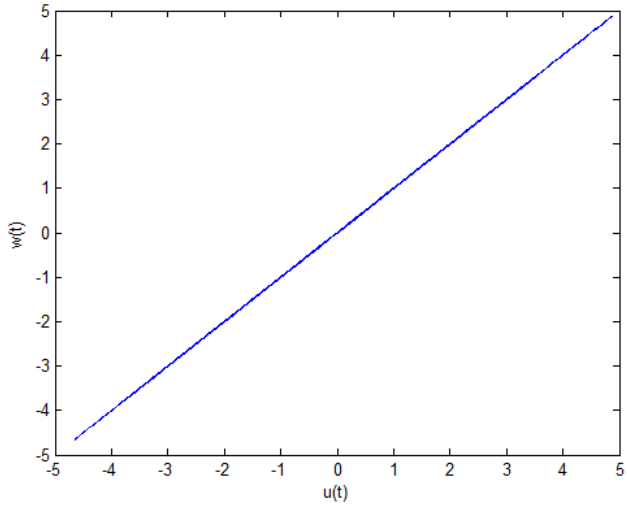

(c) Input-Output Relations with Inverse Compensation

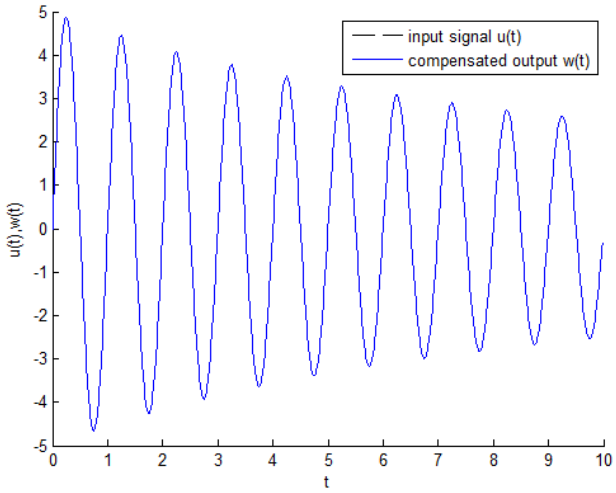

(d) $w(t)$ tracking $u(t)$

Figure 5.4: Simulation Results with $\gamma[v] = 3v$, and $u(t) = 5sin(2\pi t)/(1 + 0.1t)$

5.4 Simulation Results with Nonlinear Function

In this section, a nonlinear function $\gamma[v](t) = tanh^{-1}[0.5v]$ is chosen as the envelop functions. Thus, related functions for the inverse compensation are $\gamma'[v](t) = \frac{1}{2(1-0.25v^2)}$, $\beta[v](t) = \gamma^{-1}[v](t) = 2tanh[v]$, and $\beta'[v](t) = 2 - 2(tanh[v])^2$. Simulations in this section will verify that the mGPI model and the inverse model can characterize and compensate such a hysteresis.

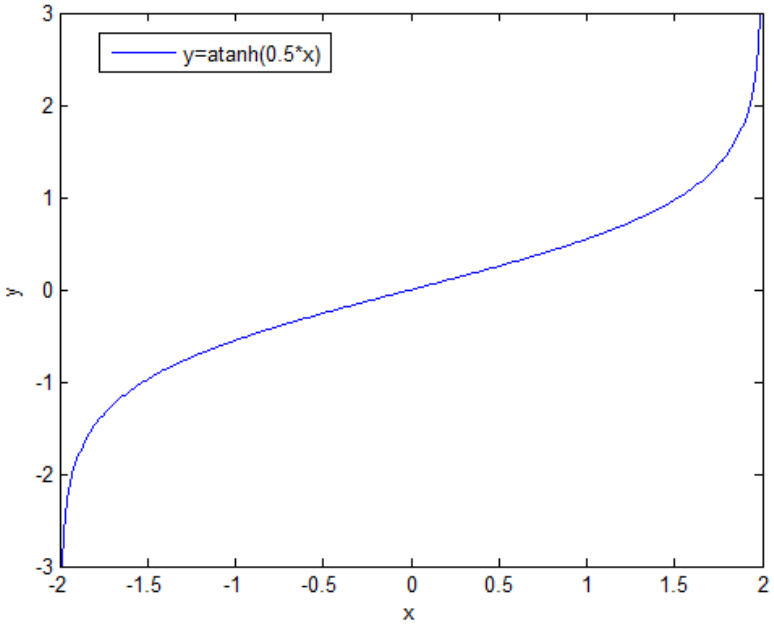

Figure 5.5: Graph of $\gamma[v](t) = tanh^{-1}[0.5v]$

As shown in Fig. 5.5, the domain of definition of $\gamma[v](t) = tanh^{-1}[0.5v]$ is ± 2. In this section, the input signals is chosen $u(t) = 0.5sin(2\pi t)/(1 + 0.1t)$, $t \in [0, 10]$. The thresholds of the 20 operators are chosen $r_i = 0.025i$. According to the inverse numerical implementation in Section 4.3, the thresholds of the 20 operators in the inverse is q_i={0.0125, 0.0253, 0.0385, 0.0519, 0.0657, 0.0798, 0.0943, 0.1090, 0.1242, 0.1396, 0.1554, 0.1716, 0.1881, 0.2050, 0.2223, 0.2399, 0.2580, 0.2764, 0.2952, 0.3144}. The Density of the 20 operators in the inverse compensator is $g(q_i)$ ={-0.0243, -0.0231, -0.0218, -0.0207, -0.0195, -0.0184, -0.0173, -0.0162, -0.0152}. As illustrated in Fig. 5.6, with nonlinear envelop functions, the feed-forward compensator can still cancel most of the hysteresis nonlinearities with limited operators.

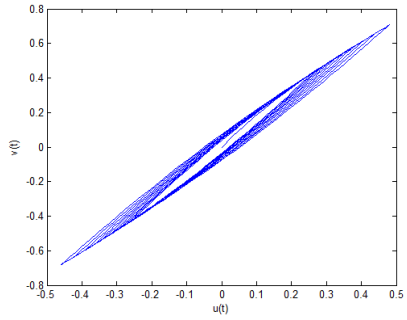

(a) Inverse Compensator

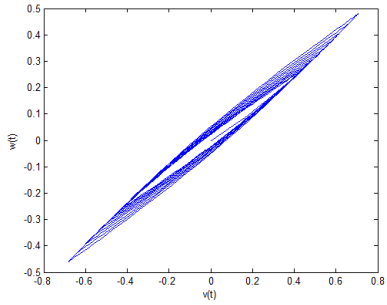

(b) Hysteresis Model

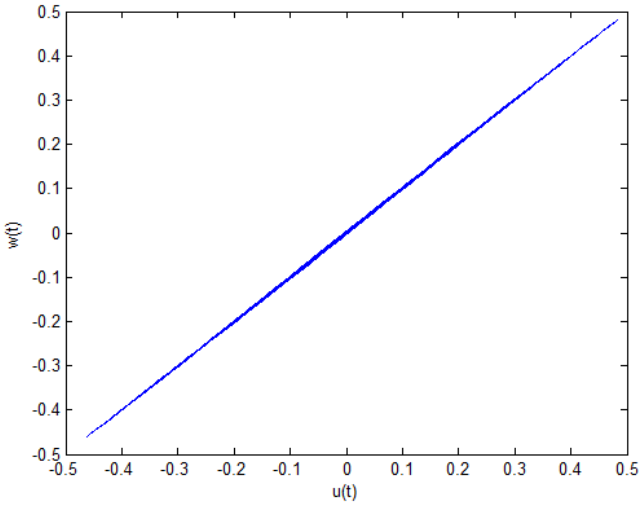

(c) Input-Output Relations with Inverse Compensation

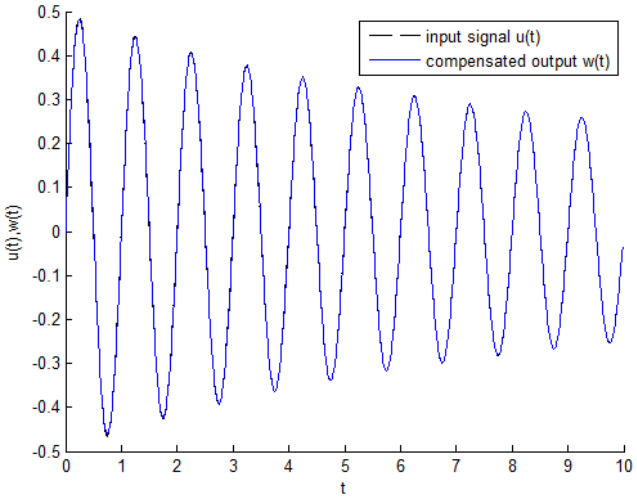

(d) $w(t)$ tracking $u(t)$

Figure 5.6: Simulation Results with $\gamma[v](t) = tanh^{-1}[0.5v]$, and $u(t) = 0.5sin(2\pi t)/(1 + 0.1t)$

5.5 Summary

In this Chapter, the proposed modefied Generalized Prandtl-Ishlinskii (mGPI) model and its inverse compensator are simulated with different kinds of envelop functions. Illustrated by the simulation results, the proposed mPGI model can precisely describe the hysteresis nonlinearities. Accordingly, the proposed inverse model can effectively compensate the hysteresis. Both models are validated in this Chapter.

Chapter 6

Conclusions and Future Work

6.1 Conclusions

The thesis focuses on the development of a modified generalized Prandtl-Ishlinskii (mGPI) model and its inverse feed-forward compensator. The hysteresis effects widely exhibit in smart material actuators, which usually worsen the controller performances, leading to oscillations or even instabilities. The thesis has comprehensibly conducted an overview of the available models and controler design methods about the hysteresis nonlinearities in the literatures. Among the available models, the Prandtl-Ishlinskii (PI) model, due to its significant analytical invertible property, has become one of the most popular hysteresis models. However, it can only describe a kind of symmetric, rate-independent, and non-saturated hysteresis, which restricts the use of the PI model.

Focusing on the PI model, the thesis proposes a modified Generalized PrandtlIshlinskii (mGPI) model, which can describe the asymmetric and saturate hysteresis. Subsequently, its inverse was derived, which can serve as feed-forward compensator. To verify the proposed mGPI model and its inverse feed-forward compensator, the simulation results were provided. The main contributions are summarized as follows,

- In Chapter 3, the restrictions of the PI model and the Generalized PrandtlIshlinskii (GPI) model are discussed. Based on these models, a modified Generalized PrandtlIshlinskii (mGPI)

model is proposed. The mGPI model can characterize a kind of asymmetric and saturated hysteresis nonlinearities, while keeping analytical invertibility property.

- Compared with the classical PI model, the proposed mGPI model can describe a more general class of hysteresis behaviors.

- In the generalized play operators in the GPI model, the threshold is no longer r, depending on the envelop functions $\gamma[v]$. Thus, the orignal meaning of the threshold r will be lost. However, in the proposed mGPI model, the threshold of the modified generalized play operators is still r.

- In the proposed mGPI model, for the bounded envelop functions, such as $\gamma[v] = tanh[v]$, the modified generalized play operator can be bounded with the same limits. Thus, the proposed mGPI model can describe the saturated hysteresis effectively. In the available GPI model,the upper and lower bounds of each operator depend on the envelop functions.

- As illustrated in Section 3.5, in the GPI model, for some envelop functions $\gamma[v]$ and threshold r, the generalized play operator will stop working. While in the proposed mGPI model, the operator works for any input.

- In Chapter 4, an analytical inverse of the proposed mGPI model is derived, which can be used as a feed-forward compensator of the hysteresis nonlinearities. The numerical implementation methods are provided subsequently. Following these steps, the parameters of the proposed inverse compensator can be calculated.

- In Chapter 5, simulation results are provided to validate the proposed inverse compensator. An identity function, a linear function, and a nonlinear function are chosen, respectively, as the envelop functions, to construct the mGPI model. The inverse compensator are constructed accordingly. Illustrated by the simulation results, the proposed model can describe the hysteresis nonlinearities and the derived inverse compensator can effectively cancel the nonlinear effects caused by the hysteresis.

6.2 Future Work

The following are suggested future studies about controller development for systems with hysteresis.

- In this thesis, the mGPI model has been proposed. But it has only been analyzed theoretically. As a future work, experimental tests will be conducted to implement the developed method together with the controller to be developed.

- In Chapter 4, the calculation of the density function of the inverse compensator includes an $\beta'(0) = (\gamma^{-1})'(0)$ in the denominator, which means the inverse compensator can not work with the envelop functions satisfying $\beta'(0) = 0$. For instance, when $\gamma[v] = v^3$, $\beta[v] = v^{1/3}$. Thus $\beta'[v] = \frac{1}{3}v^{-2/3}$, and $\beta'(0) = 0$. The proposed methods need some modification to work on these envelop functions.

- In practice, the hysteresis of the smart material based actuators are always unknown, which means in the mGPI model, the density function $p(r)$ requires being estimated as $\hat{p}(r)$. Thus, there exist compensation errors, due to the hysteresis estimation error. In the thesis, the estimation issue has not been addressed. In order to design a controller based on this inverse compensator with estimated parameters, the compensation error is required to be analyzed theoretically.

Bibliography

[1] S. O. Reza Moheimani and G. C. Goodwin. Guest editorial introduction to the special issue on dynamics and control of smart structures. *IEEE Transactions on Control Systems Technology*, 9(1):3–4, Jan 2001.

[2] G. Tao and P. V. Kokotovic. Adaptive control of plants with unknown hystereses. *IEEE Transactions on Automatic Control*, 40(2):200–212, Feb 1995.

[3] I. Mayergoyz. Mathematical models of hysteresis. *IEEE Transactions on Magnetics*, 22(5):603–608, Sep 1986.

[4] G. Bertotti and I.D. Mayergoyz. *The Science of Hysteresis: Mathematical modeling and applications*. Number v. 1 in Elsevier series in electromagnetism. Elsevier, 2006.

[5] M. Brokate. Some mathematical properties of the preisach model for hysteresis. *IEEE Transactions on Magnetics*, 25(4):2922–2924, Jul 1989.

[6] M.A. Krasnosel'skii, A.V. Pokrovskii, and M. Niezgódka. *Systems with hysteresis*. Universitext (1979). Springer, 1989.

[7] M. Brokate and J. Sprekels. *Hysteresis and Phase Transitions*. Applied Mathematical Sciences. Springer New York, 1996.

[8] P. Krejci and K. Kuhnen. Inverse control of systems with hysteresis and creep. *IEE Proceedings - Control Theory and Applications*, 148(3):185–192, May 2001.

[9] Mohammad Al Janaideh, Subhash Rakheja, and Chun-Yi Su. A generalized prandtlcishlinskii model for characterizing the hysteresis and saturation nonlinearities of smart actuators. *Smart Materials and Structures*, 18(4):045001, 2009.

[10] M. Al Janaideh, S. Rakheja, and C. Y. Su. An analytical generalized prandtl-ishlinskii model inversion for hysteresis compensation in micropositioning control. *IEEE/ASME Transactions on Mechatronics*, 16(4):734–744, Aug 2011.

[11] G. Y. Gu, L. M. Zhu, C. Y. Su, H. Ding, and S. Fatikow. Modeling and control of piezo-actuated nanopositioning stages: A survey. *IEEE Transactions on Automation Science and Engineering*, 13(1):313–332, Jan 2016.

[12] D. C. Jiles and D. L. Atherton. Theory of ferromagnetic hysteresis. *Journal of Magnetism and Magnetic Materials*, 61:48–60, 1986.

[13] Ralph C. Smith and Zoubeida Ounaies. A Domain Wall Model for Hysteresis in Piezoelectric Materials. *Journal of Intelligent Material Systems and Structures*, 11:62–79, 2000.

[14] J. Sprekels. Visintin, A.: Differential Models of Hysteresis. Berlin ctc., Springer-Verlag 1994. XI, 407 pp., 46 figs., DM 94.-. ISBN 3-540-54793-2 (Applied Mathematical Sciences 111). *Zamm-zeitschrift Fur Angewandte Mathematik Und Mechanik*, 76:144–144, 1996.

[15] Jack W. Macki, Paolo Nistri, and Pietro Zecca. Mathematical Models for Hysteresis. *Siam Review*, 35, 1993.

[16] Mohammed Ismail, Fay?al Ikhouane, and Jos Rodellar. The Hysteresis Bouc-Wen Model, a Survey. *Archives of Computational Methods in Engineering*, 16:161–188, 2009.

[17] Mohammed Ismail, Fayçal Ikhouane, and José Rodellar. The hysteresis bouc-wen model, a survey. *Archives of Computational Methods in Engineering*, 16(2):161–188, 2009.

[18] C. Y. Su, Y. Stepanenko, J. Svoboda, and T. P. Leung. Robust adaptive control of a class of nonlinear systems with unknown backlash-like hysteresis. *IEEE Transactions on Automatic Control*, 45(12):2427–2432, Dec 2000.

[19] P. Krejci. *Hysteresis, Convexity and Dissipation in Hyperbolic Equations*. GAKUTO International series. Gattötoscho, 1996.

[20] X. Zhao and Y. Tan. Modeling hysteresis and its inverse model using neural networks based on expanded input space method. *IEEE Transactions on Control Systems Technology*, 16(3):484–490, May 2008.

[21] Q. Xu. Identification and compensation of piezoelectric hysteresis without modeling hysteresis inverse. *IEEE Transactions on Industrial Electronics*, 60(9):3927–3937, Sept 2013.

[22] Ping Ge and Musa Jouaneh. Tracking control of a piezoceramic actuator. *IEEE Transactions on Control Systems Technology*, 4(3):209–216, May 1996.

[23] Xiaobo Tan and J. S. Baras. Modeling and control of a magnetostrictive actuator. In *Decision and Control, 2002, Proceedings of the 41st IEEE Conference on*, volume 1, pages 866–872 vol.1, Dec 2002.

[24] G. Song, Jinqiang Zhao, Xiaoqin Zhou, and J. A. De Abreu-Garcia. Tracking control of a piezoceramic actuator with hysteresis compensation using inverse preisach model. *IEEE/ASME Transactions on Mechatronics*, 10(2):198–209, April 2005.

[25] R. V. Iyer, Xiaobo Tan, and P. S. Krishnaprasad. Approximate inversion of the preisach hysteresis operator with application to control of smart actuators. *IEEE Transactions on Automatic Control*, 50(6):798–810, June 2005.

[26] G. Y. Gu, L. M. Zhu, and C. Y. Su. Modeling and compensation of asymmetric hysteresis nonlinearity for piezoceramic actuators with a modified prandtl-ishlinskii model. *IEEE Transactions on Industrial Electronics*, 61(3):1583–1595, March 2014.

[27] Chun-Yi Su, Qingqing Wang, Xinkai Chen, and S. Rakheja‘. Adaptive variable structure control of a class of nonlinear systems with unknown prandtl-ishlinskii hysteresis. *IEEE Transactions on Automatic Control*, 50(12):2069–2074, Dec 2005.

[28] S.A. Belbas and I.D. Mayergoyz. Dynamic programming for systems with hysteresis. *Physica B: Condensed Matter*, 306(1C4):200 – 205, 2001. Proceedings of the Third International Symposium on Hysteresis an d Micromagnetics Modeling.

[29] Fabio Bagagiolo. Dynamic programming for some optimal control problems with hysteresis. *Nonlinear Differential Equations and Applications NoDEA*, 9(2):149–174, 2002.

[30] William S. Oates and Ralph C. Smith. Nonlinear Optimal Control Techniques for Vibration Attenuation Using Magnetostrictive Actuators. *Journal of Intelligent Material Systems and Structures*, 19:193–209, 2008.

[31] Xinkai Chen, Takeshi Hisayama, and Chun-Yi Su. Pseudo-inverse-based adaptive control for uncertain discrete time systems preceded by hysteresis. *Automatica*, 45(2):469 – 476, 2009.

[32] X. Chen and T. Hisayama. Adaptive sliding-mode position control for piezo-actuated stage. *IEEE Transactions on Industrial Electronics*, 55(11):3927–3934, Nov 2008.